ADVANCED MATERIALS
www.advmat.de

# Mussel-Inspired, Self-Healing, Highly Effective Fully Polymeric Fire-Retardant Coatings Enabled by Group Synergy

*Zhewen Ma, Jiabing Feng, Siqi Huo, Ziqi Sun, Serge Bourbigot, Hao Wang, Jiefeng Gao, Long-Cheng Tang, Wei Zheng,* and Pingan Song**

**Fire-retardant coatings represent a universal cost-effective approach to providing fire protection for various substrates without compromising substrates' bulk properties. However, it has been attractive yet highly challenging to create waterborne polymeric fire-retardant coatings combining high-efficiency, generally strong adhesion, and self-repairability due to a lack of rational design principles. Inspired by mussel's unique adhesive, self-healing, and char-forming mechanisms, herein, a "group synergy" design strategy is proposed to realize the combination of self-healing, strong adhesion, and high efficiency in a fully polymeric fire-retardant coating via multiple synergies between catechol, phosphonic, and hydroxyethyl groups. As-created fire-retardant coating exhibits a rapid room-temperature self-healing ability and strong adhesion to (non)polar substrates due to multiple dynamic non-covalent interactions enabled by these groups. Because these functional groups enable the formation of a robust structurally intact yet slightly expanded char layer upon exposure to flame, a 200 µm-thick such coating can make extremely flammable polystyrene foam very difficult to ignite and self-extinguishing, which far outperforms previous strategies. Moreover, this coating can provide universal exceptional fire protection for a variety of substrates from polymer foams, and timber, to fabric and steel. This work presents a promising material design principle to create next-generation sustainable high-performance fire-retardant coatings for general fire protection.**

## 1. Introduction

It is reported that global fires caused 20600 deaths and 69500 injuries, with 83% of deaths and 61% of injuries occurring in residential buildings in 2020 (World Fire Statistics). One key reason for these building fires is the ubiquitous use of highly flammable polymer foams, e.g., polyurethane (PU), polyethylene (PE), and in particular expandable polystyrene (EPS) thermal insulation materials for buildings to create energy-saving buildings.[1] In addition to low thermal conductivity, these polymer foams are lightweight, chemical and microorganism resistant, and easy to recycle. However, their large surface area and high organic content make them inherently flammable, and when exposure to high temperatures and a flame, they can be ignited immediately. Their fires often spread rapidly and further ignite combustible materials around them, eventually triggering big fires and causing substantial losses of life and property. Meanwhile, many residential fires are reported

Z. Ma, W. Zheng
Interdisciplinary Materials Research Center
College of Materials Science and Engineering
Tongji University
Shanghai 201804, China
E-mail: zhengwei@tongji.edu.cn
J. Feng, S. Huo, H. Wang, P. Song
Centre for Future Materials
University of Southern Queensland
Springfield 4300, Australia
E-mail: pingan.song@usq.edu.au
The ORCID identification number(s) for the author(s) of this article can be found under https://doi.org/10.1002/adma.202410453



**DOI: 10.1002/adma.202410453**

Z. Sun
School of Chemistry and Physics
Queensland University of Technology
2 George Street, Brisbane 4000, Australia
S. Bourbigot
ENSCL
UMR 8207 – UMET – Unité Matériaux et Transformations
Univ. Lille
42 rue Paul. Duez, Lille 59000, France
J. Gao
College of Chemistry and Chemical Engineering
Yangzhou University
Yangzhou 225002, China
L.-C. Tang
College of Material
Chemistry and Chemical Engineering
Hangzhou Normal University
Hangzhou 311121, China

to be trigged by flammable fabric curtains or sofas, and combustible wooden furniture and building materials.[2] Therefore, it is imperative to create fire-retardant materials to mitigate residential building fires.

Fire-retardant coatings have been considered one of the most universal cost-effective approaches to creating fire-retardant materials. Generally, there are three primary strategies to impart satisfactory fire retardancy to flammable or combustible materials. Take the EPS foam as an example, one can prepare fire retardant EPS via 1) introducing flame-retardant elements during styrene polymerization, namely reactive flame retardants (FRs);[3] 2) physically blending fire retardants, i.e., capsulated FRs;[4] and 3) applying fire-retardant coatings on its surface—that is, surface FR treatment.[5] The addition of fire retardants is cost-effective but often adversely affects the synthesis of EPS and its final quality.[6] Additionally, the use of some encapsulated FRs modified with formaldehyde in EPS can pose a potential risk to human health and the environment.[4b,7] In comparison, fire-retardant coatings have multiple advantages, such as achieving a desired fire-retardant level using a very thin fire-retardant coating, retaining physical properties (e.g., color) of the coated materials, and general applications to varied substrates. Therefore, it has been highly attractive to create high-performance fire-retardant coatings.

Recently, we have developed one new type of water-based, bioinspired sulfur-containing ionic polymer coatings, poly(VS-co-HEA) or PVH and its hybrid, which endows rigid PU foam (RPUF) with an ability to self-extinguish at a coating thickness ranging from 200 to 600 µm, in addition to a strong interface adhesion.[8] Nevertheless, because of its strong polarity, such ionic polymeric fire-retardant coating shows poor adhesion to non-polar substrates, including EPS and PE. Moreover, this coating cannot self-heal at room temperature, which can compromise its long-term durability. Despite these encouraging advances, to date it has been highly challenging to develop water-based high-performance fire-retardant coatings combining high efficiency, a room-temperature self-healing ability, and strong adhesion to polar and nonpolar substrates due to a lack of rational design principles.

In nature, mussel features unique strong adhesion, self-healing, and charring due to their abundant catechol groups that have multiple dynamic physical interactions and an ability to self-crosslink to generate nonflammable char residues (see **Figure 1A**).[9] Inspired by these intriguing mechanisms, we propose a "group synergy" design strategy to engineer a new type of fully polymeric fire-retardant coating (PVHDx) via free radical copolymerization of hydroxyethyl acrylate (HEA), vinylphosphonic acid (VPA), and dopamine methacrylate (DAMA). The group synergy enables the unique combination of strong adhesion, self-healing, and high fire-retardancy in as-synthesized PVHDx coatings. Because of the presence of abundant hydroxyl and catechol groups, these coatings exhibit strong adhesion to various substrates from steel, wood, PU, and cotton to EPS and PE through multiple non-covalent interactions.[9a,10] The extensive intermolecular hydrogen bonding, the damaged PVHDx coating shows an ability to self-heal at room temperature if exposure to moisture, thus reducing the need for costly repair upon damaged.[11] More importantly, three monomers work cooperatively to generate synergistic fire-retardant effects, via the catalytic charring effect of VPA on HEA, and the self-crosslinking of catechol groups at high temperatures or in hot acidic environments created by VPA at high temperatures,[9b,12] thus leading to a robust structurally integral char layer as a fire shield, in addition to strong free radical scavenging effects of both phosphoric and catechol groups.[13] Due to the unique synergistic effect, with only 200 µm thick of coating, the treated EPS foam is nearly nonignitable, achieving a desirable UL-94 V-0 rating and a record high limiting oxygen index (LOI) up to 40.5 vol%, far surpassing existing fire-retardant strategies. Moreover, such fire-retardant coatings also exhibit exceptional fire protection for other flammable polymer foams, timber, cotton fabric, and nonflammable steel. This work offers an innovative design concept to develop next-generation fire-retardant coatings, which provide fire protection for a variety of substrates and thus hold great promise for practical applications in the fields of buildings, electronics, textiles, energy, and beyond.

## 2. Results and Discussion

### 2.1. Bioinspired Design of Fire-Retardant Coatings

Generally, water-based fire-retardant coatings show poor interfacial adhesion to non-polar polymer foams, e.g., EPS and PE because of only the presence of very weak Van der Waals forces between them.[14] In nature, because of its abundant catechol groups, mussel byssus exhibits strong adhesion to many substrates via multiple non-covalent interactions, such as hydrogen bonding, ligand bonding, cation-$\pi$ bonding, and $\pi$-$\pi$ interactions (see Figure 1A).[9c,10] In addition, the formation of crosslinked polydopamine structures in specific environments (pH = ≈1, or high temperatures)[9b,12] and their free radical scavenging activity can make an additional contribution to the optimization of the fire safety properties of the coatings.[13a,b] Figure 1B illustrates the chemical structures of the as-synthesized copolymer, PVHDx, and two control copolymers, PHD, and PVH, as well as the roles of each monomer in the copolymer coatings. Specifically, i) catechol-containing monomer, dopamine methacrylate (DAMA), contributes to the coating adhesion; ii) DAMA and film-forming monomer, hydroxyethyl acrylate (HEA) containing terminal hydroxyl groups serve as the carbon sources;[15] and iii) vinylphosphonic acid (VPA) provides fire retardancy by catalyzing the formation of carbonaceous layers at high temperatures in the condensed phase and scavenging free radicals in the gas phase.[16]

With these three monomers, VPA, HEA, and DAMA, transparent PVHD terpolymer solutions can be readily synthesized via one-step free radical copolymerization in a water/ethanol mixed medium (Figures S1,S2, Supporting Information). By tuning the molar ratio of three monomers, VPA/HEA/DAMA = (55-x)/45/x (x = 3,5,7), terpolymeric PVHD coatings with different DAMA contents are prepared to optimize adhesion and fire performance. It should be noted that the copolymerization reaction

P. Song
School of Agriculture and Environmental Science
University of Southern Queensland
Springfield 4300, Australia

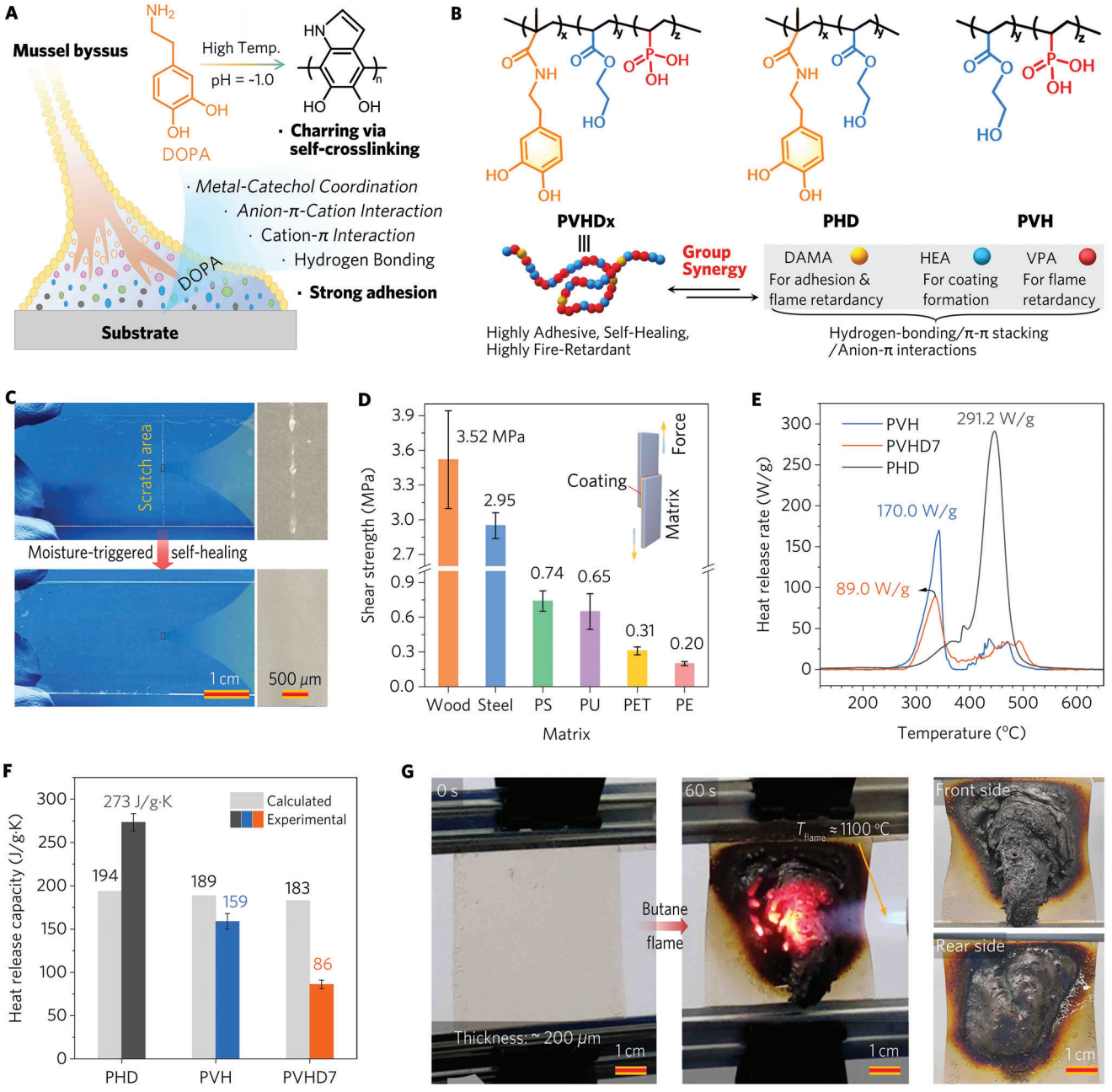


**Figure 1.** Mussel-inspired design of fire-retardant coatings enabled by group synergy. A) Schematic illustration for mussel byssus showing strong adhesion to the substrate surface, and its DOPA units have charring and self-healing abilities. B) Mussel-inspired conceptual design of highly adhesive, self-healing, and high-efficiency fire-retardant coatings enabled by group synergy. C) Photographs of the scratch-defected PVHD7 coating before and after healing. D) Shear strength of PVHD7 coating against different substrates. E) Heat release rate curves of PHD, PVH, and PVHD7 detected by microscale combustion calorimetry (MCC) system. F) Heat release capacity of PHD, PVH, and PVHD7 obtained by MCC system and MGC calculation. G) Butane flame ignition tests for evaluating the fire performance of PVHD7.

becomes unstable and tends to form gels if the content of DAMA is higher than 7%. For comparison, two binary copolymers with VPA/HEA and HEA/DAMA, designated as PVH and PHD, are prepared (Supplementary Information). The chemical structures and compositions of these copolymers are characterized by $^{1}$H nuclear magnetic resonance (NMR) (Figures S3–S5, Supporting Information) and infrared spectroscopy (IR) (Figure S6, Supporting Information). PVHD7 shows a low weight-average molecular weight ($M_w$) of 15,874 g mol$^{-1}$, due to the inhibition effect of DAMA on polymerization (Table S1, Supporting Information). In comparison, PHD exhibits the highest ($M_w$) of 234,081 g mol$^{-1}$, because of the initial formation of

phosphoric anhydride as an intermediate in the cyclopolymerization of VPA, which impedes chain extension and presents challenges in achieving high and uniform molecular weight products.[17]

Upon cast-drying, the PVHD7 copolymer forms a light yellow yet transparent film, indicating its excellent film-forming ability because of the presence of flexible HEA monomers (Figure 1G on the left). Meanwhile, because of the rigidity of DAMA, its introduction increases the glass transition temperature ($T_g$) of the final coatings, as evidenced by an increase in $T_g$ from −13.5 °C to 21.4 °C as the DAMA content increases from 0 to 5 mol% (Figure S7 and Table S2, Supporting Information). The copolymerization of soft HEA monomers and rigid VPA and DAMA monomers enables the final PVHDx coatings to be thermodynamically stable (Figures S8–S11, Supporting Information) and to readily form a thin film. More importantly, because of the formation of extensive hydrogen-bonding and other non-covalent interactions between polymer chains, as-prepared PVHDx film can readily repair at room temperature if sprayed with a small amount of water or even left in a relatively humid environment (Figure 1C). Such self-healing ability can significantly extend the lifespan of the coating. In addition, this copolymerization can potentially create additional synergistic effects between three monomers in terms of adhesion and fire performances (Figures S8,S9 and Table S2, Supporting Information).

### 2.2. Adhesive Properties of Fire-Retardant Coatings

An ideal fire-retardant coating should exhibit a strong adhesion to a variety of surfaces. To assess the adhesion of PVHDx coatings, we chose different substrates, including PS, PE, PU, polyethylene terephthalate (PET), solid wood, and steel, because they are extensively used in buildings and other fields. As presented in Figure 1D, PVHD5 exhibits varied adhesion to different substrates because of different interfacial interactions, with a shear strength against different substrates in the order: wood (3.52 MPa) > steel (2.95 MPa) > PS (0.74 MPa) > PU (0.65 MPa) > PET (0.31 MPa) > PE (0.20 MPa). Indeed, the catechol moiety in PVHDx enables adhesion to almost any surface, such as through $\pi$–$\pi$ stacking with PS and PET, and hydrogen bonding and mechanical interlocking with wood with a rough surface.[10] In comparison, a relatively weak adhesion to nonpolar PE is because there are only poor Van der Waals forces between them. Overall, this indicates that as-synthesized PVHDx shows an ability to adhere to both polar and non-polar substrates.

### 2.3. Fire Performances of Fire-Retardant Coatings

The fire performances of fire-retardant coatings themselves generally determine their fire protection capabilities. To visually examine the fire performance of as-synthesized PVHDx coatings, a cast-drying PVHD7 film with a thickness of 200 µm is flame-attacked by a butane torch with a flame temperature above 1100 °C (Figure 1G the left). Though the flame temperature is much higher than the ignition points of most organic polymers, no ignition is observed throughout the ignition process, and the coating retains its original shape after 60 s of flame attack, even if the film is loaded with a metal clamping (Figure 1G the right; Movie S1, Supporting Information). During fire testing, one can see the gradual formation of a moderately expanded, structurally integral, and thermally stable char layer, which is expected to provide effective fire protection for underlying substrates by preventing heat and mass transfer.

To further assess the fire performances of as-developed PVHDx coatings, a microscale cone calorimeter (MCC) is used. As compared to a very high peak heat release rate (PHRR) of 1161.0 W $g^{-1}$ and a total heat release (THR) of 51.0 kJ $g^{-1}$ for the organic EPS foam (Figure S12, Supporting Information), binary PHD copolymer exhibits a lower PHRR of 291.2 W $g^{-1}$ and a smaller THR of 17.3 KJ $g^{-1}$ (Figure 1E; Figure S13 and Table S7, Supporting Information). In contrast, the PVH shows smaller PHRR and THR values than the PHD. In comparison to both PHD and PVH, as-synthesized PVHD7 terpolymer demonstrates the smallest PHRR of 89.0 W $g^{-1}$ and THR of 6.7 kJ $g^{-1}$ (Figure 1E; Figure S14 and Table S7, Supporting Information), clearly showing the best fire performance of PVHD7. Interestingly, both PHRR and THR values decrease with increasing DAMA contents in the PVHD. The results also indicate a synergistic effect between the three monomers in terms of fire performance.

Theoretically, the flammability of polymers is closely related to the heat release capacity (HRC) of specific functional groups in the polymers, which has been proposed by Lyon et al.[18] The HRC of a polymer can be calculated using a molar group contribution (MGC) method Equation (1):[18]

$$HRC_{cal} = \sum_i w_i \times HRC_i \quad (1)$$

Where $HRC_{cal}$ is the calculated HRC of a polymer, $HRC_i$ reflects the contribution of group $i$ to HRC, and $w_i$ is the weight fraction of group $i$ in the polymer.

The contribution of both catechol and phosphonic groups to the HRC of PVHDx is further determined using MCC tests in conjunction with a database of MGC,[19] so theoretical $HRC_{cal}$ values of the copolymers can be calculated (Tables S3,S4 and Figure S15, Supporting Information). The HRC results clearly show a synergy between VPA and HEA, and between VPA, HEA, and DAMA (Figure 1F), but an anti-synergy between HEA and DAMA by comparing their $HRC_{cal}$ values and experimental ones (Tables S5–S7, Supporting Information). For instance, PVHD7 gives an experimental HRC of 86 J $g^{-1}$ K much lower than the theoretical 183 J $g^{-1}$ K and the difference becomes larger with increased DAMA contents, indicative of a strong synergy between VPA and DAMA monomers in terms of fire performances (i.e., HRC).

### 2.4. Room-Temperature Self-Healing of PVHDx Coating

Self-healing properties enable surface coatings to spontaneously regain their protective function after damage and to fulfill their function in damage-prone external environments.[11b] To simulate real defects, PVHD7 coating was first applied onto the glass substrate surface, then scratched with a surgical blade, followed

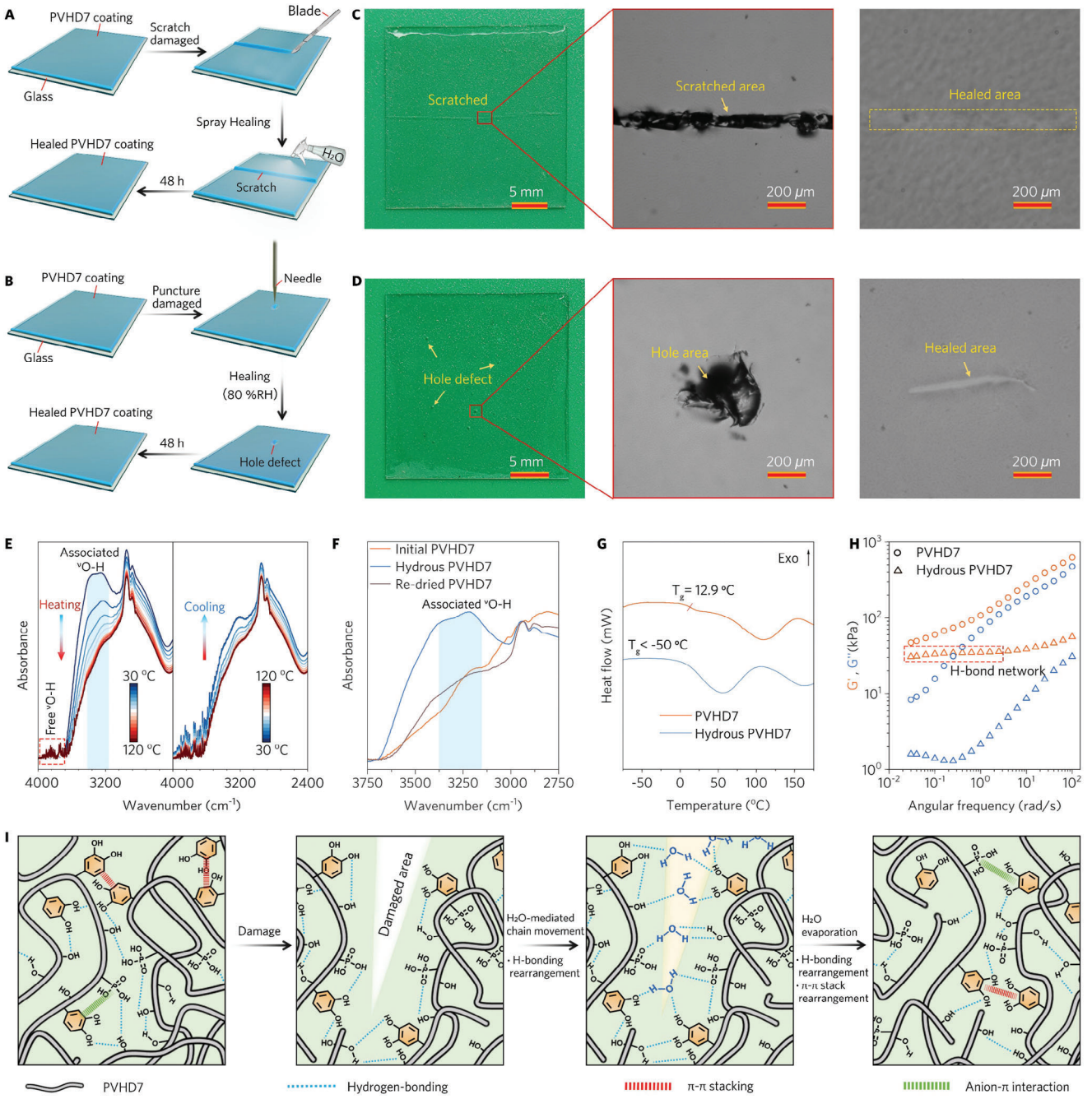


**Figure 2.** Moisture-mediated self-healing of PVHD7 coating. A) The scratch and B) perforation experiments for assessing self-healing properties. C) scratch-defected, D) hole-defected coatings, and optical microscopic (OM) images for before and after healing. E) in situ IR spectra of PVHD7. F) IR spectra of PVHD7, hydrous PVHD7, and re-dried PVHD7. G) Differential scanning calorimetry (DSC) curves and H) Dynamic rheological behaviors of PVHD7 and hydrous PVHD7. I) Schematic illustrations showing self-healing mechanisms occurring in self-healing coatings.

by moistening the defect area and left to allow itself to self-heal at room temperature (**Figure** 2A). Optical images show that the scratches completely disappear after 48 h, demonstrating its excellent self-repairing ability (Figure 2C; Figures S18,S20, Supporting Information). In addition, the coating was punctured with a tapered needle and then allowed to heal for 48 h at 80%RH, which further confirms its desired self-healing ability, as evidenced by the disappearance of holes (Figure 2B,D; Figure S19, Supporting Information).

To understand why PVHD7 coating gains such a satisfactory self-healing ability, varied temperature FTIR (VTIR) was performed by heating the coating from 30 to 120 °C, followed by cooling to 30 °C (Figure 2E). The associated $\nu_{O\text{-}H}$ intensity at 3300 $cm^{-1}$ decreases, the free $\nu_{O\text{-}H}$ intensity (3850 $cm^{-1}$)

increases slightly, and then bounces back to the initial state when the temperature increases from 30 to 120 °C and then returns to 30 °C. This indicates the breakage and dissociation of inter/intramolecular hydrogen bonding (H-bonding) as the temperature increases, resulting in the creation of free hydroxyl groups.[20] Also, the incomplete recovery of the intensity of stretching vibration peak of hydroxyl groups (O—H) during cooling is an indication of the self-condensation of part hydroxyl groups to form ether bonds. Meanwhile, when the damaged PVHD7 is exposed to high humidity, the associated $\nu_{O\text{-}H}$ peak undergoes similar intensity changes with the introduction or removal of $H_2O$ molecules (Figure 2F). Additionally, a slight red shift of the C═O peak at 1724 $cm^{-1}$ is observed (Figure S21, Supporting Information), implying an increase in the number of H-bonds, which is attributed to that H-bonds between $H_2O$ molecules and PVHD7 gradually replace those between chain segments in a humid environment.[20,21] The intermolecular H-bonding interactions between PVHD7 and $H_2O$ are further evaluated by rheological tests. A so-called "platform" of the storage modulus ($G'$) appears at a low frequency (<1 rad $s^{-1}$) (Figure 2H), indicative of the existence of an H-bonding network in hydrous PVHD7,[22] which can induce a chain rearrangement, as reflected in the fact that the decreases the $T_g$ of hydrous PVHD7 from 12.9 to below −50 °C, where the migration of PVHD7 chain segments is no longer restricted (Figure 2G). Subsequently, the volatilization of the $H_2O$ molecules leads to the re-disruption of the water-chain segment H-bonding, and the occurrence of H-bonding rearrangement and $\pi$–$\pi$ stacking rearrangement between the chain segments further facilitated the healing process (Figure 2I). In brief, the dynamic and reversible nature of the H-bonding and $\pi$–$\pi$ stacking is responsible for such a water-mediated self-healing process.

### 2.5. Application of Fire-Retardant PVHDx Coatings to EPS

To validate the fire protection capability of PVHDx, the EPS is selected as a substrate since it has been extensively used for building thermal insulation but is extremely flammable and hydrophobic. **Figure** 3A illustrates the manufacturing process of PVHD-coated EPS foam using rod-coating, with a coating thickness of less than 200 µm (Supplementary Information). Additionally, the coating surface is further treated with a silicone resin emulsion to generate a very thin hydrophobic layer to mitigate moisture and UV sensitivity (Figures 3A,B; Figure S22 and Movie S2, Supporting Information). The cross-section of PVHD7-coated EPS foam shows a bilayer microstructure with an ≈170 µm thick PVHD7 layer and an ≈1.8 µm thick hydrophobic silicone layer on the top surface. Energy-dispersive X-ray (EDX) elemental mapping confirms the uniform distribution of C, P, and N elements throughout the cross-section of the PVHD7 coating layer, while a small amount of Si element from the hydrophobic layer is mainly distributed on the topmost part of the coating (Figure 3B; Figure S24, Supporting Information).

To evaluate the adhesion of PVHDx to EPS foam, we employ the established adhesion theory that high adhesion strength is attributed to high cohesive energy density (CED) and interfacial adhesion energy (IAE),[23] which can be calculated by molecular dynamics simulations. PVHD5 shows a smaller IAE value but higher CED than both PHD and PVH, indicating its greater energy drop upon binding to EPS and superior interfacial stability, as well as higher adhesion toward EPS (Figures 3C–E). The shear strength results are in good agreement with the theoretical calculations. The shear strength of different copolymers against PS follows the order: PVHD5 (0.74 MPa) > PVHD7 (0.71 MPa) > PVHD3 (0.69 MPa) > PVH (0.51 MPa) > PHD (0.26 MPa) (Figure 3F). The presence of the dopamine-like DAMA monomers not only improves the cohesive energy of the coatings but also enhances the interfacial compatibility between the coating and EPS, as reflected by a seamless adhesion interface (Figure 3G). PVHD7 shows a slightly smaller shear strength than PVHD5, mainly because of its lower molecular weight which can weaken intermolecular interactions. The strong adhesion of PVHD5 to EPS is mainly because of the $\pi$-$\pi$ stacking interactions between benzene rings in EPS and catechol groups in PVHD5. In addition, the presence of other multiple interactions, e.g., anion-$\pi$, and hydrogen bonding between catechol, phosphonic acid, and/or hydroxyl groups, and spontaneous oxidative cross-linking behaviors also contribute to the higher CED and adhesion of PVHDx as compared to PHD and PVH (Figure 3H).[9c] Meanwhile, the adhesion results indicate a synergy between three monomers in terms of enhancing the CED of PVHDx coatings and its adhesive ability.

### 2.6. Fire Performances of Coated EPS Foam with PVHDx Coatings

Despite being an excellent building thermal insulation foam, EPS often presents a grand fire threat because it combines high flammability, low melting point, and poor char formation, making it intractable to create fire-safe EPS foam. Therefore, EPS foam is first chosen for assessing the fire protection ability of as-developed PVHDx coatings. To visually evaluate the fire protection, a homemade fire-testing setup with a digital camera and an infrared thermal imager is established to observe flame spread on a wooden cabin model (**Figure** 4A). As a result, upon exposure to butane flame, the untreated EPS foam is ignited within 1 s, then burns violently, and experiences a rapid volume shrinkage because of its porous structure and low melting point. The flame rapidly spreads to the wooden cabin, the temperature of which rapidly rises to 600 °C, and exceeds the upper detection limit of the instrument (>660 °C) in 60 s with continuous burning after the igniter removal (Figure 4B). EPS exacerbates the burning of the wooden cabin, eventually leading to only a little cabin debris left (Figure 4D).

Meanwhile, a commercially available grade B1 fire-retardant EPS (EPS-B1) is sourced and tested for comparison. The EPS-B1 shows good fire retardance since it cannot be ignited when exposed to flames of ≈1,100 °C for 8 s (Figures 4B,E). Despite this, it starts to gradually melt and eventually is ignited after 18 s of flame exposure. The flame quickly spreads to the entire exterior wall at 60 s, with the cabin eventually leaving very little residue (>660 °C) (Figure 4E; Movie S3, Supporting Information). This highlights the difficulty in reducing the flammability of EPS by traditional fire-retardant methods, especially when EPS foams are exposed to extremely high temperatures/heat fluxes. Unlike EPS-B1, the

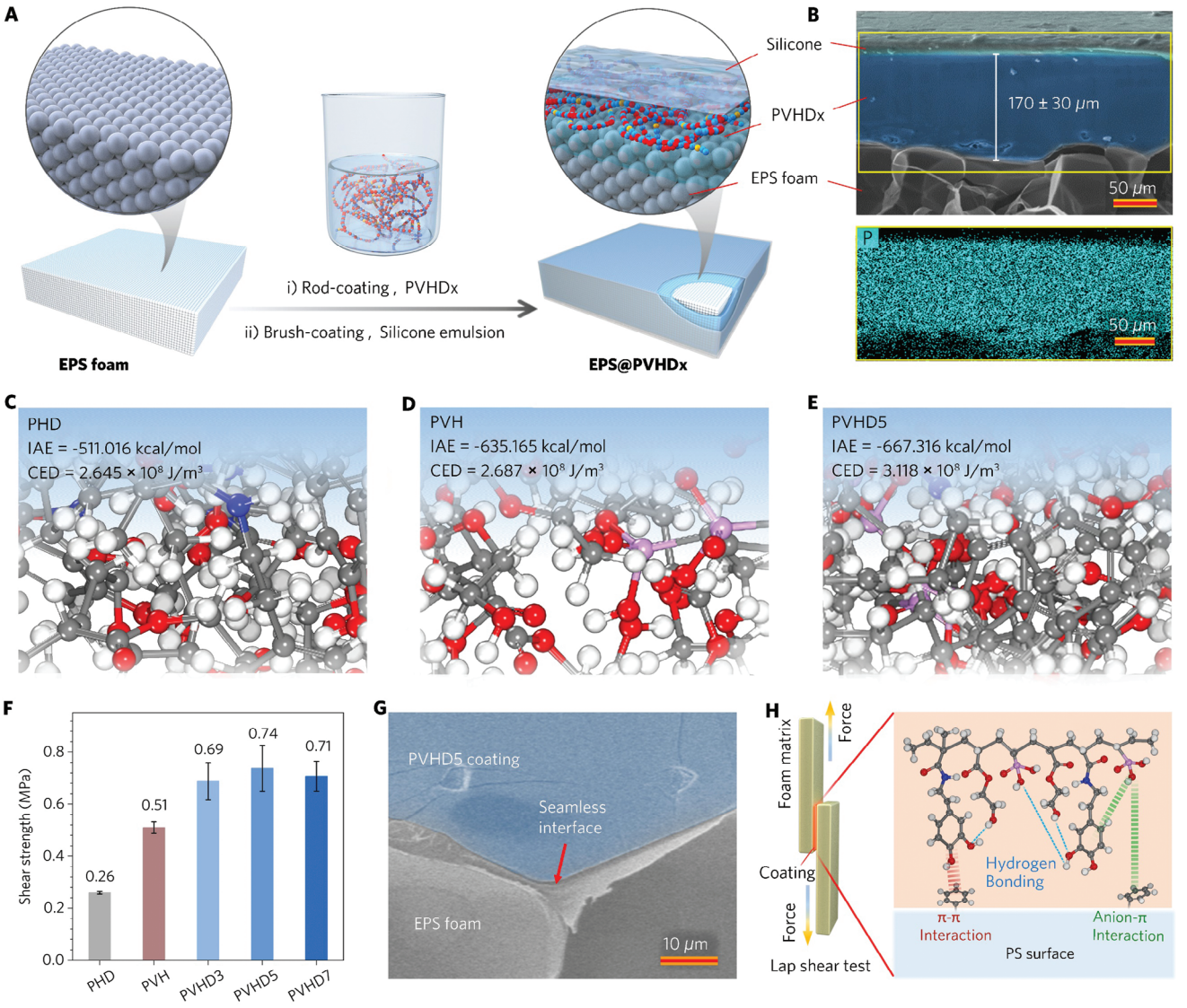


**Figure 3.** Adhesion properties of PVHDx coating. A) Illustration of the fabrication of EPS@PVHDx foam. B) Scanning electron microscopy (SEM) image for the cross-section morphology of the PVHD7-coated EPS foam along with EDX elemental mapping. C–E) Stable states, interfacial adhesive energies (IAEs), and cohesive energy densities (CEDs) of (C) PHD, (D) PVH, and (E) PVHD5 on the PS surface. F) Shear strength of coatings on PS. G) SEM image for the cross-section morphology of the PVHD5-coated EPS foam. H) Chart illustrating the adhesion or shear strength tests for foam materials.

EPS foam treated by the PVH coating does not melt even after being exposed to flame for 90 s due to the thermal protection effect of the char layer from the PVH coating (Movie S3, Supporting Information). However, because of insufficient thermal protection, the internal foam gradually softens, thus leading to thermal stress shrinkage and eventually the detachment of the char from the cabin wall.

In sharp contrast, the EPS@PVHD7 foam cannot be ignited throughout the ignition process, and thus the wooden cabin behind it only exhibits a temperature rise of 6 °C in the vicinity of the flame (Figure 4C; Movie S3, Supporting Information). Moreover, the EPS@PVHD7 foam not only retains its integral structure and size but also produces a robust intumescent char layer under the flame (Figure 4F). This char layer enables the foam to maintain its relatively steady temperature even under violent flames (≈1,100 °C), thus providing desired fire protection for the cabin behind. Meanwhile, any unfavorable phenomenon, such as buckling and detachment, is not observed, further highlighting the exceptional fire performances of EPS@PVHD7 foam and fire protection of PVHD7.

In addition, since the PVHD7 coating can be scaled up for production, a large-size EPS@PVHD7 foam (35 × 30 × 5 $cm^3$) is manufactured to further evaluate its fire performance (Figure 4G). Likewise, the large foam can withstand a violent flame strike when exposed to a flame temperature of up to 1100 °C for ≈30 s, without generating bright flames and volume shrinkage (Figure 4H; Movie S6, Supporting Information). The macrostructure of the foam remains unchanged, despite a small area of heat diffusion occurring from the

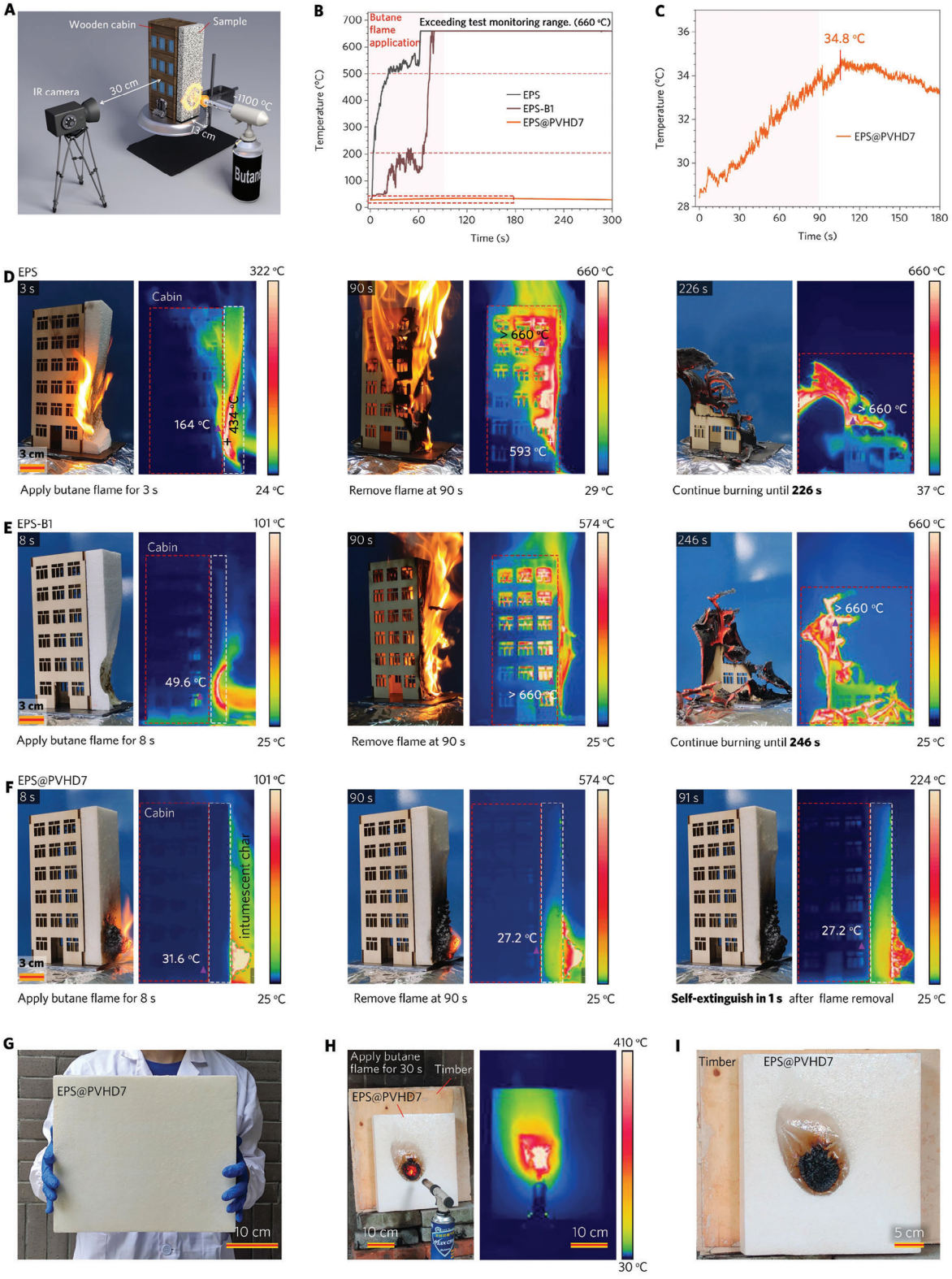


**Figure 4.** Coated EPS foam exhibits a fire-extinguishing capability. A) The homemade setup for assessing fire behaviors. B,C) Maximum temperature of the cabin protected by (B) EPS, EPS-B1, and (C) EPS@PVHD7 foams during the test as a function of burning time. D–F) Digital images for the burning behavior of the cabin protected by (D) EPS, (E) EPS-B1, and (F) EPS@PVHD7 under the butane flame for 90 s, along with their side temperature variation with time determined by the IR camera. G) Digital photograph of large-scale EPS@PVHD7 foam of ≈1050 $cm^2$ area. H) Digital photograph (Left) and infrared thermal imaging (Right) of the ignition process of large-scale EPS@PVHD7 when it was burned by a butane flame for 30 s. I) Digital photos of large-scale EPS@PVHD7 after two consecutive 30 s ignitions.

ignition point (Movie S6, Supporting Information). In contrast, upon exposure to flame, the EPS foam shows a long violent burning (>6 min), ultimately leading to significant fire damage to the underlying timber (Movie S4, Supporting Information).

Apart from a qualitative visual evaluation of fire performances, several quantitative assessments, such as LOI, vertical burning tests, and cone calorimetry testing are also conducted on PVHDx coatings. The PVHD7-coated EPS foam achieves a high LOI of up to 40.5% and a satisfactory UL-94 V-0 rating, as compared to an LOI of 18.0% and no rating during vertical burning testing for untreated EPS foam (Figures S25,S26 and Table S7, Supporting Information). This further shows that EPS@PVHD7 is highly fire-retardant and can meet stringent fire-retardancy requirements for its application as a building thermal insulation material.

Compared with LOI and vertical burning testing, cone calorimetry is a more powerful tool for assessing the real burning behaviors of materials under forced fire scenarios, because it can provide more key fire parameters, such as time to ignition ($t_{ign}$), HRR, smoke production rate (SPR), and CO production (COP). Under an external heat flux of 35 kW m$^{-2}$, the $t_{ign}$ of virgin EPS and EPS-B1 are 50 and 59 s, respectively (Table S8, Supporting Information). Their long $t_{ign}$ values are not because of their good fire retardance, but because, before ignition under external radiation, their melting and shrinkage enlarge the distance between the foam surface and the cone heater.[5b,24] Upon ignition, EPS, and EPS-B1 reach their PHRR values of 529 kW m$^{-2}$ at 79 s ($t_{PHRR}$) and 370 kW m$^{-2}$ at 99 s, respectively (**Figure 5A**). In contrast, EPS@PHD shows a shorter $t_{ign}$ but a significantly longer time to PHRR ($t_{PHRR}$) of 127 s relative to EPS (Table S8, Supporting Information).

In comparison, both EPS@PVH and EPS@PVHD7 achieve ultralow PHRR values, which are 83% and 87% lower than that of virgin EPS, respectively (Figure 5A). The PVH coating expands slowly when exposed to heat radiation until it collides with the ignition gun, which causes the char to rupture and the ignition of the underlying foam, followed by an impermanent burning (less than 10 s) (Movie S7, Supporting Information). In contrast to the PVH coating, the PVHD7 coating can form a more robust char layer since it contains more polyDAMA segments. More importantly, as an antioxidant, the catechol group in PVHDx can significantly interrupt the ignition process by scavenging active HO· radicals,[13a,b,25] one of the unstable strong oxidizing radicals involved in the free radical chain reaction in the gas phase during combustion,[2b] thus allowing EPS@PVHD7 to give a very long $t_{ign}$ of 445 s, indicative of strong anti-ignition ability of the PVHD7 coating.

Meanwhile, two important fire parameters, fire performance index (FPI) and fire growth index (FGI) calculated by Equations (2,3), are introduced. Larger FPI and smaller FGI values generally indicate better fire retardancy and lower fire risk. Untreated EPS exhibits a small FPI of 0.095 m$^2$s kW$^{-1}$ but a large FGI of 6.69 kW m$^{-2}$ s$^{-1}$, indicating its serious fire risk. In contrast, most of the coatings increase FPI values of the foams to varying degrees and all of them dramatically reduce FGI values. Specifically, the FPI and FGI values of EPS@PVHD7 are 6.45 m$^2$s kW$^{-1}$ and 0.12 kW m$^{-2}$ s$^{-1}$, respectively, 68-fold and 1.8% than that of untreated EPS, and 40-fold and 2.6% than that of commercial EPS-B1 foam, further highlighting the better fire retardance and lower fire risk of PVHD7 (Figure 5B).

$$FPI = \frac{t_{ign}}{PHRR} \tag{2}$$

$$FGI = \frac{PHRR}{t_{PHRR}} \tag{3}$$

$$TRP = q_{ex}\sqrt{t_{ign}} \tag{4}$$

$$t_{ign} = \frac{b}{q_{ex} - q_{crit}} \tag{5}$$

Another key metric, the thermal response parameter (TRP), reflects a material's ignition delay under external heat flux Equation (4) and is also used for evaluating fire performances. EPS@ PVHD7 gives a far higher TRP value of 738 s$^{1/2}$ kW m$^{-2}$, tripling that (247 s$^{1/2}$ kW m$^{-2}$) for highly flammable EPS foam, further indicating the anti-ignition ability of EPS@PVHD7 (Table S8, Supporting Information). In addition, the minimum heat load required for the ignition of EPS foam can be quantitatively evaluated by the critical heat flux ($q_{crit}$) according to Equation (5). In Equation (5), b is the fitting constant and $q_{crit}$ represents the minimum value of heat flow to ignite a substance. The $q_{crit}$ for EPS@PVHD7 is 34.8 kW m$^{-2}$, much higher than 18.8 kW m$^{-2}$ of the pristine EPS and 8.0 kW m$^{-2}$ of EPS@PVH. This means that the as-developed PVHD7 coating can act as an exceptional fire shield by enhancing the anti-ignition ability of the underlying flammable substrates in most fire scenarios (Figure 5C; Table S9, Supporting Information).

It is reported that ≈80% of deaths in building fires are caused by the inhalation of smoke and toxic gases,[26] and thus the control of SPR and CO production is crucial. The uncoated EPS foam exhibits a high average specific extinction area (ASEA) value of 684.6 m$^2$ kg$^{-1}$, bringing about a peak SPR (PSPR) value up to 0.15 m$^2$ s$^{-1}$. Despite a certain fire retardance, EPS-B1 releases more smoke during burning (745.8 m$^2$ kg$^{-1}$ for ASEA and 0.22 m$^2$ s$^{-1}$ for PSPR). In contrast, both ASEA and PSPR of EPS@PVHD7 respectively reduce to 251.9 m$^2$ kg$^{-1}$ and 0.049 m$^2$ s$^{-1}$, 63% and 67% lower than that of EPS foam, respectively (Figure 5D; Table S8, Supporting Information). Moreover, EPS@PVHD7 also shows appreciable reductions in peak CO production (PCOP) and peak $CO_2$ production ($PCO_2P$), a decrease of 59% and 77%, respectively, compared to those of EPS (Figure 5E; Table S8, Supporting Information). The significant smoke suppression of PVHD7 is mainly attributed to its superior charring ability, which facilitates the formation of an integral protective layer to prevent the thermal decomposition and burning of the internal EPS (Table S8, Supporting Information).

To highlight the merits of the terpolymer PVHD7 coating, the PHRR reduction, prolonged ignition time, and LOI value of EPS@PVHD7 are compared with those of previously reported fire-retardant EPS foams in Figure 5F, with detailed fire performances and preparation methods listed in **Table 1**. Encapsulation of PS masterbatch with fire retardants before foaming is the existing dominant approach for making fire-retardant EPS

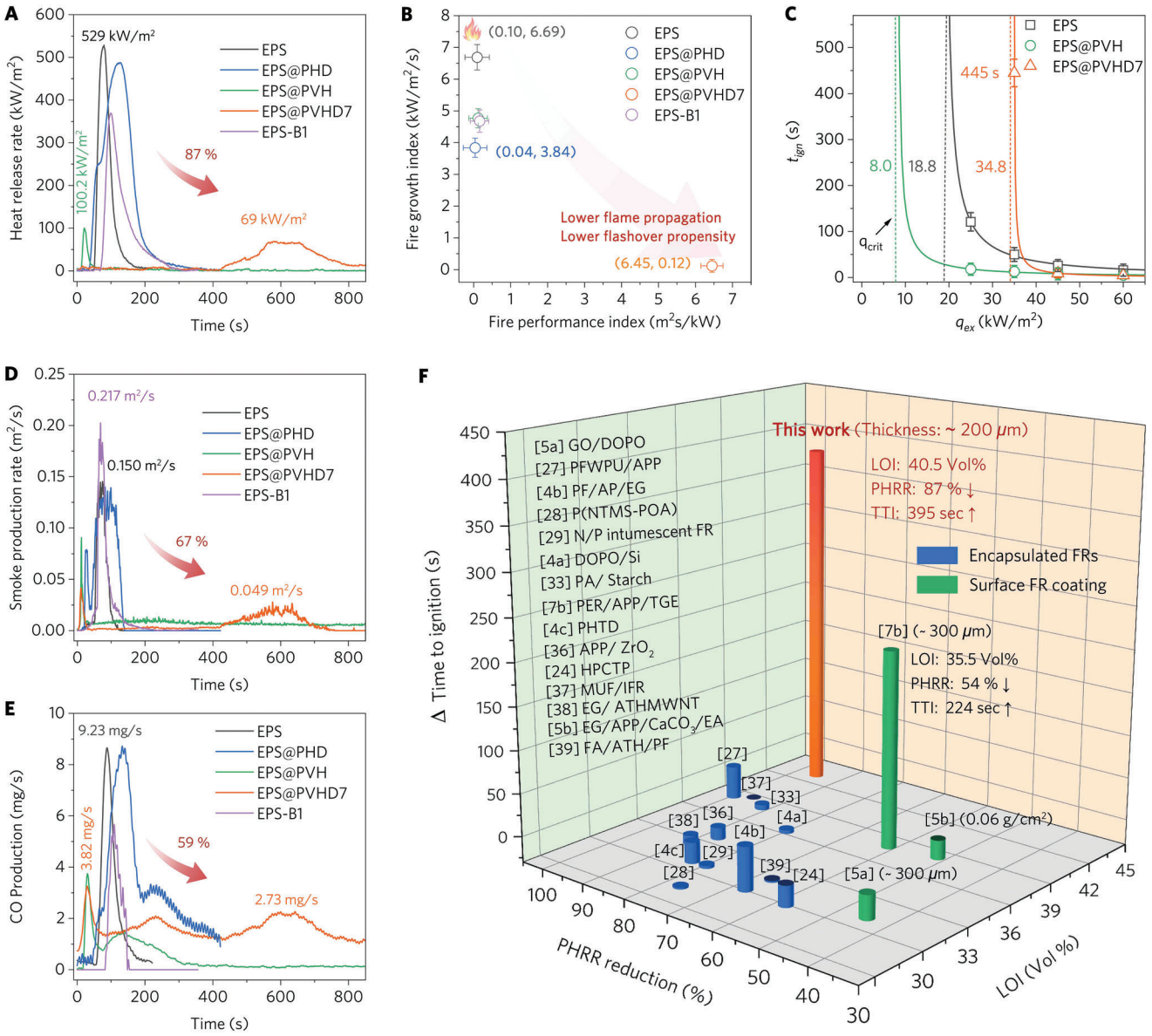


**Figure 5.** Coated EPS foam exhibits enhanced fire-retardant performances. A) HRR curves, B) FPI and FGI, C) $t_{ign}$, and the fitted $t_{ign}$ curves plotted with respect to $q_{ex}$ for foam samples. D) SPR curves. E) CO production plots. F) Comparisons of LOI, PHRR reduction, and prolonged $t_{ign}$ between as-designed EPS@PVHD7 with other existing fire-retardant EPS foam counterparts.

foam. However, this method usually fails to prevent the melting of EPS at high temperatures. Almost all encapsulated fire-retardant EPS systems do not show extended time to ignition ($t_{ign}$). Only a few surface FR coatings, such as a phenolic epoxy resin (PER)/ammonium polyphosphate (APP)/functionalized graphene (TGE) coating, with a thickness of 300 um, can delay the $t_{ign}$ by 224 s.[7b] However, this system is still inferior to as-developed PVHD7 coating, as evidenced by a $t_{ign}$ extension of 395 s at a coating thickness of only 200 μm. Moreover, the PVHD7-coated foam achieves an unprecedented LOI of 40.5 vol%, far superior to previous counterparts, in addition to a substantial reduction in PHRR (−87%).

Some encapsulated fire retardants, e.g., fire-retardant polyurethane foam (PFWPU)/APP[27] and melamine-urea-formaldehyde resin (MUF)/intumescent flame retardant (IFR),[37] provide comparable reductions in PHRR (91% and 88%, respectively). However, because of their limited efficiency, a very high loading level (above 60 wt%) is usually required to endow the final foam with desired fire retardancy, which often increases the difficulty in the foaming process and the deterioration of the mechanical properties of the final foams. Another drawback of the encapsulation method is the difficulty of recycling the foam after use.

Overall, PVHD7 coating is superior to previous fire-retardant approaches in terms of improving LOI values and anti-ignition ability and reducing heat and smoke release of EPS. Moreover, PVHD7 coating combines multiple

**Table 1.** Comparison of fire performances of as-designed fire-retardant EPS foam with previous counterparts.

| FR systems | Refs. | LOI | PHRR [kW/m$^2$] | PSPR [m$^2$ s$^{-1}$] | $t_{ign}$ (s) | UL-94 rating | Method |
|---|---|---|---|---|---|---|---|
| PVHD7 | This work | 40.5% | 69 (−87%) | 0.025 (−82%) | 445 (+395) | V-0 | Coating |
| GO/DOPO | [5a] | 29.0% | 304.6 (−38%) | – | 31 (+28) | V-0 | |
| EG/APP/$CaCO_3$/EA | [5b] | 37.7% | ~250(−50%) | – | 17 (−23) | V-0 | |
| PER/APP/TGE | [7b] | 35.5% | 201.4(−54%) | 0.039(−55.2%) | 227 (+224) | V-0 | |
| PFWPU/APP | [27] | 35.8% | 53.8(−91%) | – | 41 (+38) | V-0 | Encapsulated |
| PF/AP/EG | [4b] | 28% | 115(−60%) | 0.063(−52.3%) | 52 (+50) | V-0 | |
| ATH/PF | [7a] | – | 121(−82%) | – | 16 (+11) | – | |
| P(NTMS-POA) | [28] | 26.5% | 215(−68.8%) | – | 6 (+2) | V-0 | |
| N/P intumescent FR | [29] | 28.8% | 188(−71.6%) | 54(−70%) | 5 (+3) | V-1 | |
| APSC | [30] | 35.2% | 316(−52.6%) | 0.3(−73%) | – | V-0 | |
| MDI/IFR | [31] | – | 57.6(−81%) | – | – | – | |
| EMF/MCAPP | [32] | 31.4% | 173(−81.5%) | – | – | V-0 | |
| DOPO/Si | [4a] | 34.0% | 163.9(−72%) | 0.16(−20%) | 5 (+4) | V-0 | |
| PA/ Starch | [33] | 35.5% | 107(−83%) | 0.1(−73%) | 18 (+6) | V-0 | |
| RP/EG | [34] | 26.9% | 181 (−72.9%) | 0.15(−86%) | – | V-0 | |
| PHTD | [4c] | 28.8% | 226.1(−74.9%) | 0.05(−77.3%) | 27 (+24) | V-0 | |
| MPP/EG | [35] | 33.5% | 197 (−71%) | 0.04(−84%) | – | V-0 | |
| APP/ $ZrO_2$ | [36] | 31.5% | 179(−79%) | – | 15 (+14) | V-0 | |
| HPCTP | [24] | 29.6% | 169(−56.9%) | – | 14 (−25) | V-0 | |
| MUF/IFR | [37] | 36.3% | 49(−87.9%) | – | 4.2 (−0.2) | V-0 | |
| EG/ ATHMWNT | [38] | 30.3% | 177(−81%) | – | 4.8 (+10) | V-0 | |
| FA/ATH/PF | [39] | 29.6% | 120(−59.9%) | 0.017(−66%) | 8 (−2) | V-0 | |
| EG | [3b] | 31.3% | (−77%) | – | – | V-0 | Reactive |

advantages, such as facile synthesis, green solvent, high transparency, self-healing ability, strong adhesion, and outstanding fire retardancy (Figures S18,S22,S23, and S26, Supporting Information), thus holding great promise for massive production and many potential industrial applications.

### 2.7. Fire-Retardant Mechanism of PVHDx Coatings

It is of great significance to elucidate the fire-retardant actions of PVHD7 coating on EPS foam. Theoretically, phosphorus/nitrogen-rich fire-retardant coatings function by not only diluting flammable gases but also releasing phosphorus-containing free radical species to inhibit chain reactions via quenching active free radicals in the gas phase. For this reason, we first employ thermogravimetric analysis-infrared spectrometry (TG-IR) to determine gaseous pyrolysis products. EPS shows a main decomposition temperature of 400–500 °C in $N_2$ condition, and its decomposition products exhibit strong absorption signals of hydrocarbons, such as benzene rings and =C—H groups at 3074 and 1498 cm$^{-1}$ (Figures S28,S29, Supporting Information). It indicates that EPS mainly degrades to aromatic monomers, dimers, aromatic heterocyclic groups, etc.[29] In contrast, all coatings show attenuated absorption peaks despite an earlier pyrolysis. Apart from the signals of carbonyl compounds (1762 cm$^{-1}$), both PVH and PVHD7 show non-combustible $CO_2$ (2358 cm$^{-1}$) and P—O (950 cm$^{-1}$) fragments, which can dilute the fuels and interrupt the chain reaction in the gas phase (Figure S28, Supporting Information). In addition, the weakest IR signal of PVHD7 indicates its highest charring ability.

Unlike in $N_2$, EPS undergoes a more complete oxidative decomposition in air conditions. The absorption peaks located at 3072, 1496, and 692 cm$^{-1}$ correspond to benzene rings, and those at 1632, and 910 cm$^{-1}$ belong to the stretching of C—C bonds and bending vibrations of —$CH_2$ at 420 °C, indicating the initial decomposition of EPS (**Figure 6**A).[4a] A clear and persistent $CO_2$ signal (2351 cm$^{-1}$) is also detected and does not disappear until 800 °C (Figure 6A). In comparison, PHD shows two intense outgassing phases at 550 and 622 °C, respectively, attributed to the decomposition of polyHEA and polyDAMA segments (Figure S29D1, Supporting Information). The combination of VPA and DAMA monomers inhibits the gas release of coating, raising the major pyrolysis temperature of PVHD7 to 770 °C. Notably, carbonyl-derived gases disappear and only $CO_2$ gases are released, which can slow and even terminate the combustion (Figures 6B,C).

To understand the flame inhibition effect of PVHDx coatings in the gaseous phase, the flame inhibition effect is quantified by Equation (6), where EHC is the effective heat of combustion obtained from cone calorimetry.[40] EPS@PVHD7 shows a flame inhibition effect of 55%, much higher than 28% of EPS@PVH (Table S10, Supporting Information), further confirming a

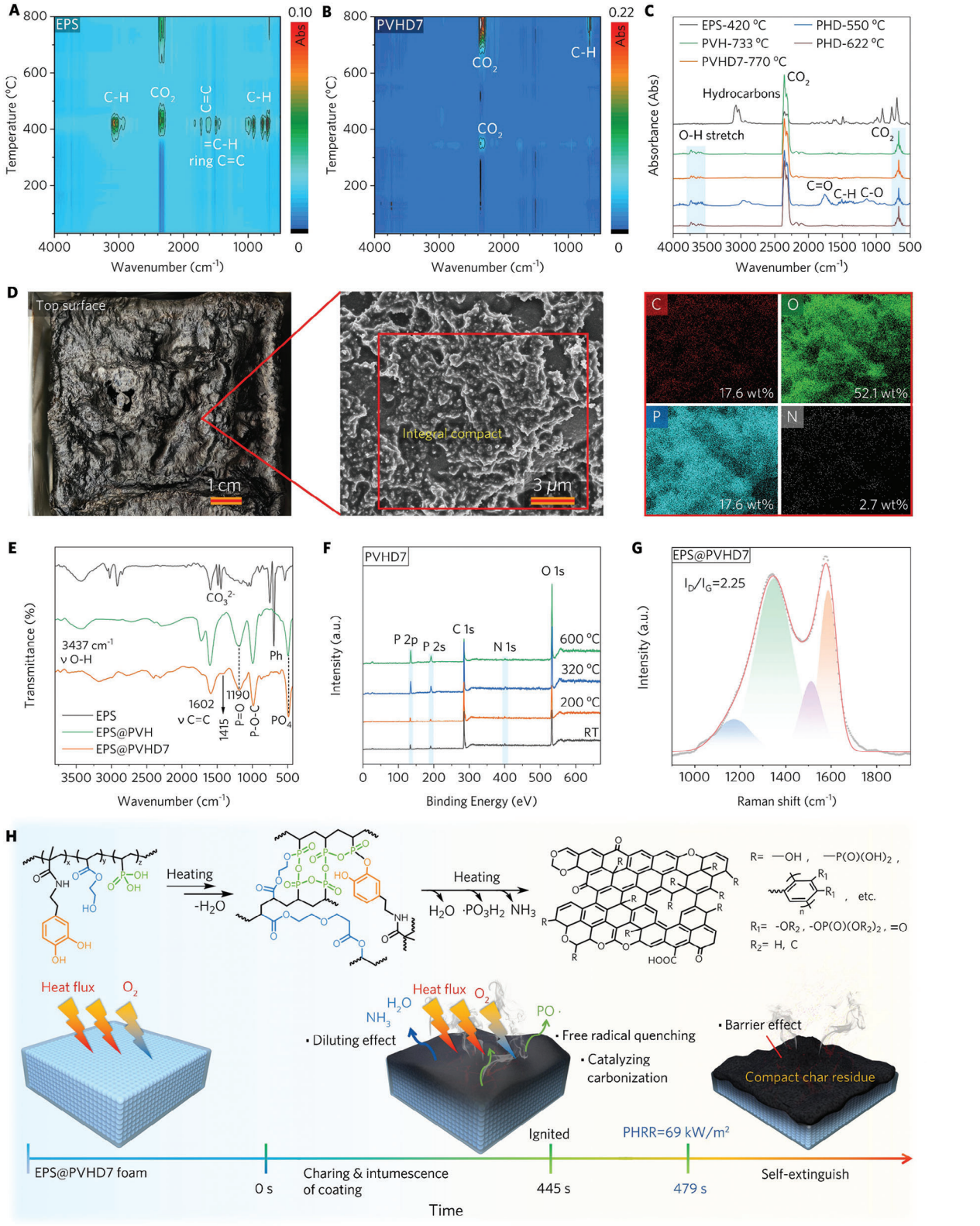


**Figure 6.** Modes of action of PVHD7 coating. A,B) In situ FT–IR spectra of evolved gases for (A) EPS, and (B) PVHD7 coating. C) FT–IR spectra of gaseous products of EPS and various coatings at their violent decomposition temperatures. D) Digital and SEM images and EDX mappings of the top surface for the char from EPS@PVHD7 after cone testing. E) FT–IR spectra of char residues for EPS, EPS@PVH, and EPS@PVHD7. F) XPS results of PVHD7 before and after various high-temperature conditions. G) Raman spectra of EPS@PVHD7 after cone test. H) Schematic illustration for the combustion as a function of temperature for EPS@PVHD7.

synergistic flame inhibition effect between polyDAMA and polyVPA.

$$\text{Flame inhibition effect} = 1 - \frac{EHC_{\text{coated foam}}}{EHC_{\text{foam}}} \quad (6)$$

$$\text{Charring effect} = 1 - \frac{TML_{\text{coated foam}}}{\text{TML}_{\text{foam}}} \quad (7)$$

$$\text{Barrier protective effect} = 1 - \frac{\text{PHRR}_{\text{coated foam}}}{\text{PHRR}_{\text{foam}}} / \frac{\text{THR}_{\text{coated foam}}}{\text{THR}_{\text{foam}}} \quad (8)$$

Besides a gas-phase mechanism, theoretically, surface fire-retardant coatings often act in the condensed phase due to their high char yields and ability to form an integral char layer when exposed to heat fluxes. According to Equations (7,8), the charring effect of EPS@PVHD7 reaches 35%, with a barrier protective effect of up to 86% (Table S10, Supporting Information), which implies the high charring ability and excellent thermal protection of the char layer derived from PVHD7 coating.[40] This can be reflected by a more integral and thicker char layer for all coated foams except EPS@PHD (Figure S30, Supporting Information), in contrast to no residues left for both EPS and EPS-B1 after cone tests. Microscopically, EPS leaves a fragmented char residue with a porous and loose microstructure at high magnifications (Figure S31A,A1, Supporting Information). In sharp contrast, EPS@PVHD7 leaves a highly compact interact char residue without any pores (Figure 6D; Figure S31C,C1, Supporting Information). Additionally, a uniform distribution of element P (17.6 wt%) from polyVPA, and elements C (17.6 wt%) and O (52.1 wt%) in the selected area is determined (Figure 6D). It is noteworthy that element N is also determined, implying that the dopamine moiety in the coating participates in the charring process.

Furthermore, we probe the chemical compositions of the top surface of chars. The FT-IR spectrum of the EPS foam char shows absorption peaks at 3450 $cm^{-1}$ ($\nu$O—H), 1066 $cm^{-1}$ ($\nu$C—OH), 1604 and 696 $cm^{-1}$ (benzene ring),[8a] indicative of a carbonaceous layer (Figure 6E). In contrast, these absorptions cannot be detected in the char of EPS@PVHD7, suggesting that the top char layer is largely derived from PVHD7. Meanwhile, the catalytic carbonization of phosphonate groups in PVHD7 results in the generation of a phosphorus-rich carbonaceous layer, as confirmed by new peaks for P—O-C at 989 $cm^{-1}$ and P═O at 1190 $cm^{-1}$.[7b] A characteristic peak at 1415 $cm^{-1}$ attributed to the C═N group generated by the DAMA monomer appears at elevated temperatures (Figure 6E; Figure S17, Supporting Information).[9b] These results further prove the key role of PVHD7 in the condensed phase. Raman spectra of char residues show their area ratios of D to G peak ($I_D/I_G$) values in an order of EPS (2.47) > EPS@PVH (2.38) > EPS@PVHD7 (2.25), indicating that the presence of VPA and DAMA enhances the graphitization degree of the char (Figure 6G; Figure S32, Supporting Information).

X-ray photoelectron spectroscopy (XPS) is further used to reveal elemental compositions of the chars (Figure S33, Supporting Information). Compared to PHD, elemental P is determined in the chars of PVH and PVHD7. The signal of N 1s is detected in PVHD7 even after heating treatment at 600 °C in air, indicating the formation of a P/N/C hybridized char layer (Figure 6F). First, the ratio of O 1s to C 1s increases slightly with increasing temperature, while the content of P 2p increases significantly (Figure 6F). It further indicates the lower thermal stability of hydrocarbon chain segments dominated by polyHEA in PVHD7, and the gradual transformation of the PVHD7 coatings from a carbonaceous layer to a more stable phosphorus/carbonaceous layer. There is only a tiny decrease in the content of N, implying that only part of elemental N is also involved in the char formation by oxidative cross-linking of the dopamine analogs. In addition, the deconvolution of the high-resolution C 1s spectrum proves the existence of several functional groups, e.g., C═C (284.6 eV), C—C (285.0 eV), C—O and C—N (286.3 eV), and O—C═O (288.8 eV) (Figure S34, Supporting Information). The gradual disappearance of O═C—O with increasing temperatures further proves the degradation of polyHEA segments. The appearance of a binding energy peak at 290.0 eV is caused by $\pi$–$\pi^*$ excitation affected by emitted electrons.[41] This suggests that the thermal stability and thermal transition behavior of polyDAMA segments play a crucial role in the condensed phase.

Based on the above comprehensive analysis, a possible mode of action for as-designed PVHD7 is proposed (Figure 6H). Upon exposure to external heat flux, dehydration reactions first occur between hydroxyl, phosphate, and catechol groups in the terpolymer, leading to the formation of a stable cross-linked network. With increasing temperatures, the breaking of chemical bonds results in the release of volatile gas products, primarily non-combustible gases (e.g., water vapor, $CO_2$, and $N_2$) and·$PO_3H_2$ free radicals,[16b] which can inhibit the flame in the gas phase by diluting fuels/oxygen and interrupting chain reactions, and contribute to the volumetric expansion of the char layer. With a further increase in temperature, the polyHEA segments undergo dehydration and cyclization in the presence of phosphoric acid derived from polyVPA. Meanwhile, the polyDAMA segments undergo oxidative cross-linking promoted by phosphoric acid, which improves the quality of the char layer. A mechanically robust, slightly expanded, structurally integral char layer is eventually created after multiple-step complicated chemical reactions. Such char layer can effectively block heat and mass transfer as well as oxygen permeation, thus providing desired fire protections for the underlying substrates, e.g., EPS.

### 2.8. Anti-Aging of PVHDx Coatings and their Impact on the Thermal Conductivity of EPS

Though surface-treated foams are not always used in an environment directly exposed to sunlight, it is still necessary to evaluate their anti-aging ability. Both EPS and PVH-treated EPS demonstrated an excellent UV-resistant ability, as evidenced by their unaltered colors and morphologies after 96 h of UV-accelerated aging tests (Figures S35,S36, Supporting Information). In comparison, no significant changes in microstructure and morphology are determined though the color of PVHDx coatings becomes slightly yellow and deepens with increasing DAMA contents (Figures S35–S37, Supporting Information). This means that as-prepared PVHDx coatings possess

a good anti aging ability. In addition, because of a much higher thermal conductivity ($\lambda$) of 0.342 W $mK^{-1}$, the presence of as-developed PVHD7 coatings increases the $\lambda$ of EPS to 0.0390 W $mK^{-1}$ (Figure S38, Supporting Information), which still meets the value required for building thermal insulation materials.

### 2.9. General Applications of PVHDx Coatings to Various Substrates

To explore the general fire protection of as-developed PVHD7 coating, we select several other representative flammable polymer foams (PU, PET, PE), solid wood, and cotton fabrics, as well as noncombustible steel plates. Because of a reliable adhesion to these substrates (Figure 1D), the PVHD7-coated foams can be readily manufactured (Figure S40, Supporting Information).

As-developed PVHD7 coating can also provide these flammable polymer foams with exceptional fire protection. PU foam exhibits a short $t_{ign}$ of ca. 11 s and a high PHRR of 306 kW $m^{-2}$ at 63 s (Table S13, Supporting Information). In contrast, the coated PU foam forms a solid char layer on the foam surface and its $t_{ign}$ and $t_{PHRR}$ are prolonged to 33 and 1247 s, respectively, with a very small PHRR value of only 61 kW $m^{-2}$, reducing by 80% (**Figure 7A**), in addition to a significant reduction in smoke release (Table S13, Supporting Information). The protection of PVHD7 coating significantly reduces the thermal degradation of PU and thus increases the char residue (Figure 7B) and the formation of an intact and compact protective char layer, relative to a porous, loose residue for virgin PU (Figure 7C). Meanwhile, PVHD7 provides similar fire protection for both PE and PET foams and even endows them with a self-extinguishing ability (Figures S41,S42, Supporting Information). This highlights its general fire protection applications for nearly all polymeric foams.

Solid wood has been widely used as building materials but also presents potential fire hazards, as highlighted by the recent Notre-Dame de Paris fire. Compared with untreated wood, the treated wood, wood@PVHD7, shows a significant delay in $t_{ign}$ from 110 to 214 s, indicative of an improved anti-ignition ability (Table S13, Supporting Information). Meanwhile, wood exhibits two HRR peaks, indicating its two-step combustion feature (Figure 7D). The first peak is more important because it represents a critical window for occupant evacuation in a building fire. The treated wood, wood@PVHD7, exhibits a very small 1st PHRR (ca. 36 kW $m^{-2}$), a 73% reduction relative to the control wood. Also, all smoke parameters are decreased to different extents (Table S13, Supporting Information). This is attributed to the higher residual char yield (24.0 wt%, 16-fold of uncoated wood) of wood@PVHD7 (Figure 7E) and the intact char layer derived from PVHD7 (Figure 7F).

Flexible substrates, such as cotton fabric, have been widely used as architectural decorative and curtain materials. Its fire-retardant treatment can be carried out by simply immersing the fabric into the PVHD7 coating solution followed by air-drying. As-developed PVHD7 coating can offer a similar satisfactory fire protection for cotton fabrics. The untreated fabric gives a high PHRR value of 217 W $g^{-1}$ and a high THR value of 16.6 kJ $g^{-1}$ due to its inherent flammability (Figure 7G; Table S14, Supporting Information). In comparison, the treated fabric, cotton@PVHD7, shows significant decreases in both PHRR and THR. Meanwhile, cotton fabrics can be ignited within 3 s upon exposure to a flame, followed by a continuous vigorous burning until it burns out completely, after the ignition source removal (Figure 7H). In contrast, the cotton@PVHD7 can self-extinguish within 5 s after torch removal and retain its intact shape (Figure 7I), thus achieving a UL-94 V-0 rating (Movie S8, Supporting Information). These results fully suggest the excellent fire protection of PVHD7 for cotton fabric and other flammable fabrics.

In addition to the above flammable organic materials, we further assess the thermal protection of our PVHD7 coating for load-bearing steel. Because the mechanical strength of steel is extremely sensitive to temperature and often drops by 30%–50% above 400 °C,[42] thus tending to trigger an instantaneous collapse of the steel structure. A homemade testing set-up is built to evaluate the thermal protection of PVHD7 for steel, and thermocouples are used to record the top surface temperature (TST) of the tested steel plates when the bottom side of which is exposed to a vigorous butane flame (>1400 °C) (Figure 7J). When exposed to the flame, the TST of the bare steel rapidly increases from room temperature to 400 °C within 127 s and reaches 485 °C at 240 s. In contrast, the TST of the PVHD7-coated steel rises more sluggishly with increasing exposure time, reaching a steady 400 °C until 400 s, and maintaining 120 °C lower than that of the bare steel (Figure 7K; Movie S9, Supporting Information). Such good thermal protection is largely due to the great adhesion of the coating to the steel as well as the thermal barrier effect of the char layer derived from PVHD7 (Figure 7L). Therefore, the as-prepared PVHD7 coating holds great potential providing for satisfactory thermal protection for steel structures in real scenarios.

## 3. Conclusion

In this study, we report a bioinspired, self-healing, highly adhesive, highly effective fully polymeric fire-retardant coating based on the proposed "group synergy" design principle. The As-created fire-retardant coating exhibits a rapid moisture-trigged self-healing ability and strong adhesion to various polar and non-polar substrates. It can provide exceptional fire/thermal protection from a variety of substrates, such as flammable polymer foams (e.g., EPS, PU, PE, PET), timber, cotton fabric, and steel. With only a 200 µm-thick coating, the coated EPS foam can resist ignition and self-extinguish immediately. In addition to a desired UL-94 V-0 rating and a high LOI value of 40.5%, the treated EPS foam shows a significantly improved anti-ignition ability, an ultralow PHRR value of 69 kW $m^{-2}$ (reduced by 87%), and a PSPR value of 0.049 $m^2$ $s^{-1}$ (reduced by 67%), compared to the control EPS foam, making it far surpass commercial B1 grade fire-retardant EPS, and previously reported fire-retardant EPS counterparts. Such exceptional fire performances are mainly attributed to the positive synergistic effect between phosphonic, catechol, and hydroxyethyl groups that lead to the formation of an intact compact char layer in the condensed phase, in addition to their free radical scavenging effect in the gas phase. Moreover, PVHDx coatings show an insignificant impact on the thermal

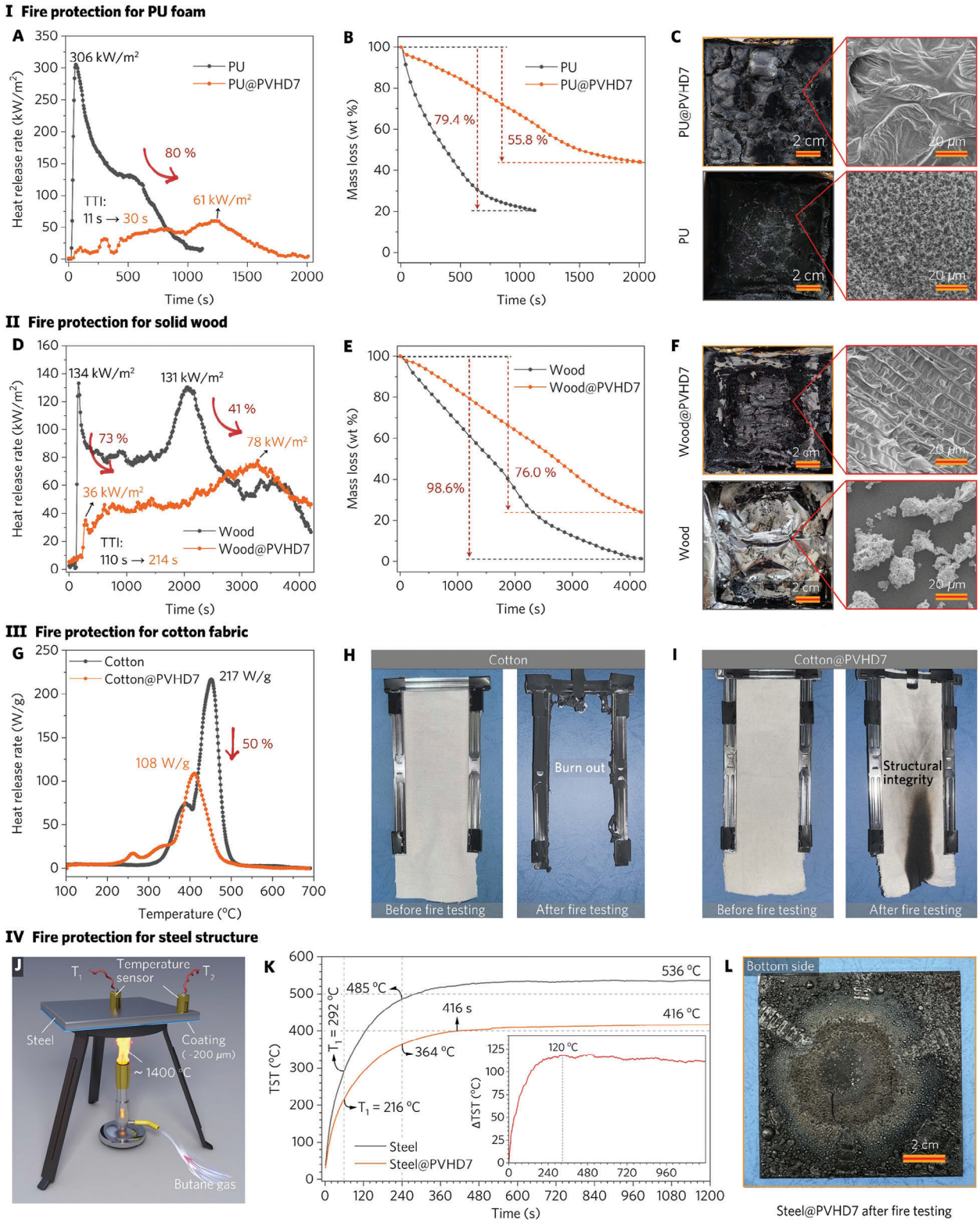


**Figure 7.** The PVHD7 coating offers general fire protection. A) HRR curves, B) Mass loss curves, C) Digital photographs (left) and SEM images (right) for the char residues of PU and PU@PVHD7 foams. D) HRR curves, E) Mass loss curves, F) Digital photographs (left) and SEM images (right) for the char residues of solid wood and PVHD7-coated wood. G) HRR curves of cotton and PVHD7-soaked cotton fabrics detected by MCC system. H,I) Digital image of VFT test: (H) cotton fabric, and (I) PVHD7-soaked cotton fabric. J) The homemade setup for determining the TST of steel plates. K) The TST of steel sheet, and steel@PVHD7 and the TST difference (△TST) between bare and coated steel specimens as a function of heating time. L) Digital photograph of steel@PVHD7 after fire testing.

insulation of EPS foam, which can be accurately predicted by theoretical calculations. Thus, as-developed fire-retardant coating can provide universal fire protection for a wide range of materials including polymer foams, timber, fabrics, and steel structures. This work provides a promising material design principle that helps expedite the development of fire-safe coatings and materials for extending their applications in the areas of construction, transportation, pipelines, electronics, and beyond.

## 4. Experimental Section

*Materials*: Vinylphosphonic acid (VPA, >95%) and 2-hydroxyethyl acrylate (HEA, 99%) were purchased from Shanghai Macklin Biochemical Co., Ltd., China. 2-(3,4-Dihydroxyphenyl) ethylamine hydrochloride (DOPA, 98%), 2,2′-azobis(2-methylpropionamidine) dihydrochloride (AIBA, 98%) and methacrylic anhydride (95%) were obtained from Anhui Senrise Technologies Co., Ltd, China. Sodium tetraborate decahydrate (99%) and sodium bicarbonate (99%) were supplied by Bide Pharmatech Co., Ltd, China. Hydrochloric acid was purchased from Sinopharm Chemical Reagent Co., Ltd, China. Ethanol (>99.9%), tetrahydrofuran (THF, >99.9%), ethyl acetate (EA, >99.5%), and hexane (>97%) were purchased from Shanghai Titan Scientific Co., Ltd, China. Dialysis bags of 1000D were obtained from Shanghai Yuanye Bio-Technology Co., Ltd., China. Expandable polystyrene (EPS, density: 22 kg $m^{-3}$) foam and commercial fire-retardant EPS foam (EPS-B1, density: 22 kg $m^{-3}$) were supplied by Shenzhen Lehao Building Materials Co., Ltd., China. Polyethylene terephthalate (PET) foam was supplied by Jiangsu Yueke New Material Co., Ltd, China. Polyethylene (PE) foam was supplied by Shanxi Miaoyao Building Materials Co., Ltd., China. Wood (China fir) was supplied by Xiangfa Timber Processing Factory., China. Cotton fabrics (100%, 315 g $m^{-2}$) were supplied by Yifang Textiles Co., China. Steel (Q235) was provided by Xinghua Zhongzhiyuan Stainless Steel Products Co. Ltd., China. Silicone resin emulsion (Melonbean-9712) was obtained from Melonbean Innovative Welt GmbH, Friedberg, Germany. All chemicals were used as received without further purification.

*Polymerization and Characterization of Poly(Vinylphosphonic Acid-Co-2-Hydroxyethyl Acrylate-Co-Dopamine Methacrylate) (PVHDx)*: Here, a representative synthesis of the PVHD7 was described. purified HEA (5.0 g, 43 mmol), VPA (5.2 g, 45.8 mmol), and AIBA (0.09 g) were stirred in a mixed solvent of deionized water (33.9 g) and ethanol (4.5 g) in a 100 mL closed round bottom flask, and the mixture was bubbled with $N_2$ for 30 min. DAMA (1.48 g, 6.7 mmol) dissolved in ethanol (10 g) was added dropwise to the above solution within 10 min. The obtained solution was then heated to 60 °C and stirred under $N_2$ atmosphere for 24 h for polymerization. The as-obtained crude product consisted of the main copolymer product and by-products of lower molecular weight polymers. Subsequently, by-products and excess solvents were removed by dialysis, followed by concentration under reduced pressure to the desired concentration for further coating applications. The purified ternary copolymer coating can be obtained by precipitation and collection in acetone, followed by vacuum drying at 30 °C, for further characterization (Figure S44, Supporting Information). Likewise, both PVHD3 and PVHD5 were synthesized with different initial VPA: HEA: DAMA feed ratios based on the above process. The chemical structures and compositions of these copolymers were characterized by Fourier transform infrared (FT–IR) spectra and $^1$H NMR using $D_2O$ as the solvent. The VTIR was carried out using a VERTEX 70v spectrophotometer (Bruker, Germany) under a nitrogen atmosphere in the range of 1100–4000 $cm^{-1}$, and the PVHD7 coating was applied on ZnSe substrate and heated from 30 to 120 °C at 1 °C $min^{-1}$. The weight-average ($M_w$), number-average ($M_n$) molecular weights and polydispersity (PDI) of PHD were obtained by a gel permeation chromatograph (GPC, PL-GPC120) eluting with DMF, whereas PVH, PVHD5, and PVHD7 were eluted with $H_2O$. Dynamic frequency sweeps of PVHD7 and hydrous PVHD7 were performed on a rheometric expansion system at room temperature at a frequency range of 0.03–100 rad $s^{-1}$ under a strain of 1% in the linearity region. Scanning electron microscopy (SEM) and energy dispersive X-ray spectrometry (EDX) measurements were performed to characterize the morphology and composition of PVHD7 coating using a field emission scanning electron microscope (SU8010) at an accelerating voltage of 5.0 kV. Before the test, the specimen surfaces were coated with a thin-layer gold.

*Thermal Analysis*: A differential scanning calorimeter (TA Discovery DSC 250) was used to determine the glass transition temperature ($T_g$) values of coatings. Approximately 3.0 mg of the specimen was enclosed in an aluminum pan, and nitrogen was used as the protective gas at a flow rate of 50 mL $min^{-1}$. Coatings were heated from 20 to 70 °C at a rate of 10 °C $min^{-1}$, kept isothermally for 10 min before being quenched to −80 °C and then heated to 180 °C at a rate of 5 °C $min^{-1}$. The data were obtained from the second heating scan. Thermogravimetric analysis (TGA) tests were performed on a TG 209F3 thermogravimetric analyzer (NETZSCH, Germany). Typically, 5–10 mg of specimens was heated from room temperature to 800 °C at a heating rate of 20 °C $min^{-1}$ under air and nitrogen atmosphere. The TGA results indicate that the copolymer coatings exhibit higher char yields than EPS foam in $N_2$ conditions (Figures S8,S11, Supporting Information). The PHD copolymer shows an increased initial degradation temperature ($T_i$) ≈269 °C and a relatively reduced char yield of 7.9 wt% (Table S2, Supporting Information), because of its good thermal stability but low charring ability from the polyHEA segment. In contrast, the presence of the phosphorus-rich monomer VPA can provide flame retardancy at lower temperatures ($T_i$ < 173 °C) and facilitate suppressing the decomposition of polyHEA segments at ≈440 °C (Figure S8B, Supporting Information). For PVHD7 coating, the involvement of DAMA in an acidic environment optimizes the thermostability of the coating, evidenced by its elevated $T_i$ and char residues (40.0 wt%) compared to PVH (Figure S8A, Supporting Information).

Since fire-retardant coatings often work in air atmosphere, it is more important to investigate their thermal oxidation degradation behaviors in air. EPS still exhibits a single-step decomposition behavior because of its charring feature, but the $T_{max}$ is significantly advanced by ≈80 °C and almost no residue is left ultimately (Figure S11, Supporting Information). Additionally, the $T_i$ of the binary copolymer PHD is reduced by 43 °C compared to that in $N_2$ (Table S2, Supporting Information) due to the lack of flame-retardant elements and stable structures. In contrast, the $T_i$ of PVHD7 is delayed by ≈17 °C (Figure S9A, Supporting Information), presumably due to the oxidative polymerization of the polyDAMA segment in the copolymer with the involvement of acid and oxygen, accompanied by the optimization of its early thermal stability. On the other hand, the char yield of binary copolymer PVD reaches 25 wt%, despite its inferior film-forming performance (Figure S10, Supporting Information). Throughout the entire heating process, the mass loss of PVH remains consistently lower than those of all terpolymer coatings, demonstrating the synergistic flame-retardant effect between DAMA and VPA. All the coatings undergo secondary degradation above 700 °C, attributed to the poor heat resistance of the polyVPA segment in the air (Table S2 and Figure S9B, Supporting Information).

*Fire Testing*: Microscale combustibility tests were carried out on a microscale combustion calorimetry (MCC) system (Govmark, Model MCC-2, USA). Typically, ≈8 mg of the coatings or EPS were heated from 100 to 650 °C at a heating rate of 1 °C $s^{-1}$ with nitrogen/oxygen (80/20, volume ratio) gas mixture. The limiting oxygen index (LOI) was obtained by a JF-3 oxygen index instrument (Jiangning, China) with a sample size of 100 × 10 × 10 $mm^3$ according to ISO4589-2:1996. The UL-94 vertical burning test was undertaken using a 5402H-V BURNING TESTER instrument and the sample had a size of 130 × 13 × 10 $mm^3$ according to ASTM D 3801. A Cone Calorimetry Test (CCT) was carried out on an FTT UK device according to ASTME1354 and ISO 5660. PU, PE, PET, and wood specimens (100 × 100 × 30 $mm^3$) were tested at a heat flux of 35 kW $m^{-2}$, and EPS specimen (100 × 100 × 30 $mm^3$) was tested at the heat fluxes of 25, 35, 45 and 60 kW $m^{-2}$. The thermographic images were captured using an infrared thermal camera (FLIR E85) with a thermal sensitivity of ≤2%. The thermal protection tests were carried out by burning Q235 steel (100 × 100 × 2.5 $mm^3$) protected on one side by PVHD7 coating in a butane-air mixture flame, and the temperature change on the

back side of the steel (unprotected) was monitored in real-time using a thermocouple.

*Fire-Retardant Mechanism*: Thermogravimetric analysis-infrared spectrometry (TG–IR) was used to investigate the gas-phase fire-retardant mechanism of the coatings, carried out on a thermogravimetric analyzer (DT-50) coupled with a Fourier transform infrared spectrometer (170SX) from 25 to 800 °C at a heating rate of 20 °C $min^{-1}$ under nitrogen and air atmosphere. X-ray photoelectron spectroscopy (XPS) testing was performed on an ESCALAB250 (ThermoVG, USA) spectrometer using Al Ka (1486.6 eV) radiation with a passage energy of 15 mA and 12 kV. Raman spectra were recorded on a Dilor SA spectrometer with an argon laser line at 514.5 nm.

*Thermal Conductivity Measurement*: Thermal insulation is a crucial indicator in the practical application of EPS foam. Here, two infrared thermography cameras were set up to detect the top and side surface temperatures (TST and SST) of the foam on a hot table at 80 °C (Figure S38C, Supporting Information). The TST of EPS increases rapidly by 3.5 °C within 2 min and reaches 35.1 °C at 30 min (Figure S38E, Supporting Information). The TST then fluctuates within a small range due to external environmental disturbances and remains generally stable until 60 min, indicating its good insulation properties. In contrast, the coated foams with any of the as-synthesized four coatings exhibit similar temperature increases, and both TST and SST show similar trends to those observed for the neat EPS, indicating the insignificant impact of the copolymer coatings (Figure S38D, Supporting Information). Thermal conductivity ($\lambda$) was used to quantitatively characterize the thermal insulation properties of coated EPS foams at different temperatures, and small foam specimens with dimensions of $5 \times 5 \times 3$ $cm^3$ were prepared for testing. The $\lambda$ of the foam and film samples was performed on a DRL-III thermal conductivity tester using 20 mW output power in the transient mode at a relative humidity of 50 ± 10%. The temperature and humidity chamber were used to store the sample for a minimum of 24 h at 25 °C and 50% humidity before measurement. The $\lambda$ values for all foams increase with rising test temperature (Figure S38B and Table S12, Supporting Information). The $\lambda$ of the coated EPS foam is slightly higher than that of pure EPS because of the higher $\lambda$ value of the coating (0.3420 W $m^{-1}$ K), but it is still at an acceptable level (≤0.04 W $m^{-1}$ K) due to the thin thickness of the coating.

The $\lambda$ of the surface-coated bulk material depends mainly on the combined effect of the foam body, the top/bottom coatings, and the four side coatings. Therefore, an equation is used to predict the value of $\lambda$, as shown in Equation (9):

$$\lambda_{\text{coatedfoam}} = \frac{2t_{\text{coat}}\lambda_{\text{coat}}}{t_{\text{total}}} + \frac{t_{\text{foam}}\lambda_{\text{foam}}}{t_{\text{total}}} + 4\xi\lambda_{\text{coat}} \quad (9)$$

$$t_{\text{total}} = 2t_{\text{coat}} + t_{\text{foam}} \quad (10)$$

$$\xi = \frac{t_{\text{coat}}}{t_{\text{foam}}}, (t_{coat} << t_{\text{foam}}) \quad (11)$$

Where $t_{coat}$ and $t_{foam}$ refer to the thicknesses of the coating (≈200 µm) and the underlying foam bulk (here, 3.0 ± 0.1 cm), $\lambda_{coat}$ and $\lambda_{foam}$ are the thermal conductivity of the coating and the foam respectively, and $\xi$ is a geometric parameter determined by the $t_{coat}/t_{foam}$ ratio (≪1).

Overall, this method can accurately calculate the $\lambda$ values that are close to the experimental ones (Figure S38A and Tables S11,S12, Supporting Information). For EPS@PVHD7 foam, the calculated $\lambda_{\text{coated foam}}$ values exhibit a consistent variation with experimental data with the temperature transform (Figures S38A,B, Supporting Information).

According to the commercial specifications given by Sto Corp., as an example, the thickness of EPS insulation boards for actual building applications ranges from 19 to 305 mm. The effect of a 200 µm-thick coating on the $\lambda$ value of the larger samples was evaluated according to Equation (9). Regardless of the coatings or temperatures, the integrated thermal conductivity gradually converges to $\lambda_{foam}$ value with the increase of $t_{foam}$ (Figure S39, Supporting Information). This further provides theoretical support for the nearly negligible negative impact of the ultra-thin PVHD7 coating in practical large-scale applications.

*Water Resistance Tests*: Water resistance is another critical factor for the practical applications of fire-retardant coatings. Though as-prepared PVHD copolymers are water soluble due to the presence of abundant hydrophilic hydroxyl groups (—OH) in the chemical structures, the coating turns insoluble in water more upon drying at 70 °C which is the temperature for drying all coated samples. Specifically, the heat-dried PVHD7 at 70 °C cannot re-dissolve in water even with prolonged stirring and further sonication, and only a slight swelling was observed (Figure S45, Supporting Information). This is primarily because of the self-condensation of some hydroxyl groups in the copolymer during the heating process, leading to a slight self-cross-linking of the dry polymer coating, which thus shows insolubility in water.[43] This can be verified by the VTIR testing of PVHD7. As compared with the dry film dried at 30 °C, the PVHD7 film that was heated up to 70 °C shows a significant reduction in the intensity of the stretching vibration ($\nu_{O-H}$) of hydroxyl groups, clearly indicating that part hydroxyl groups in the copolymer are consumed (Figure S46, Supporting Information).[44] Meanwhile, the increase in the relative total intensity of the absorption peak of both P═O and C—O—C groups implies the formation of new ether groups as a result of the self-concentration of O—H groups. Another visual evidence is that a 1 mm-thick PVHD7 film dried at 70 °C could retain its initial shape without redissolving in water despite some swelling and cracking after being soaked in water for 72 h (Figure S47, Supporting Information).

Despite its water insolubility, the dry PVHD7 coating surface can still become sticky when exposed to air for some time depending on the relative humidity of the environment due to its hygroscopic or moisture sensitivity. Therefore, to address its moisture sensitivity, a thin hydrophobic silicon coating is applied to the PVHD7 coating surface to improve its water resistance (Supplementary Information). Without silicone-treatment, the dry coating suffers severe swelling and deformation upon being rinsed with flowing water for 25 min or being immersed in water for over 45 min (Figures S48,S50 and Movie S10, Supporting Information). In comparison, the silicone-treated EPS@PVHD7 can withstand its shape and structural integrity without any changes (Figures S49,S50 and Movie S11, Supporting Information), clearly demonstrating its good water resistance. As-developed fire-retardant PVHD coatings can be mainly used with some typical materials, including polymeric insulation foams, structural steel and timber (in buildings), and fabric curtains, which are often used indoors, rather than directly exposed to outdoor conditions. This means that the coatings are less likely to undergo these harsh water-attack scenarios, such as water rinsing, and immersion in their practical applications.

*Mechanical and Adhesive Strength Measurements*: The shear adhesion strength was evaluated by using a SANS universal testing machine (CMT 6000) according to the standard ASTM F2255. The coatings were placed between two substrates (Steel, PE, PET, PS, PU, and wood) with an overlapping area ($20 \times 10$ $mm^2$), and a stretching rate of 10 mm $min^{-1}$. The compressive test was performed at a rate of 25 mm $min^{-1}$ using a SANS universal testing machine (CMT 6000) according to ISO604-2002.

*UV Resistance Tests*: The UV aging experiment was carried out by exposing the foam samples under an UV lamp (distance: 5 cm) with a power of 20 W and an UV wavelength of 313 nm. The morphologies of the samples with different irradiation times were observed by digital photographs (Figure S35, Supporting Information) and microscopically (Figure S36, Supporting Information). Their chemical structures were recorded by an FT–IR spectrometer (Figure S37, Supporting Information).

*Molecular Dynamics Simulations*: To investigate the cohesive energy density of adhesive copolymers and the interfacial interactions with the PS surface, corresponding energies were calculated. Molecular dynamics simulations had been performed in the Forcite tool in Materials Studio.[45] First, several initial models were built by using the Amorphous Cell module in Materials Studio. Then, to bring the system to equilibrium, the system was separately optimized for energy and geometry. Finally, 10,000 PS of NVT simulation at 298 K was performed to relax the polymer structure and achieve system equilibrium. A nose thermostat was used to control the system temperature. All simulations were performed with a CAMPASSIII force field.[46] In addition, the mean square displacement and diffusion coefficient was calculated based on molecular dynamics.

## Supporting Information

Supporting Information is available from the Wiley Online Library or from the author.

## Acknowledgements

This work acknowledged the National Natural Science Foundation of China (No. 22301220), the Shanghai Pujiang Program (22PJ1413900), the Fundamental Research Funds for the Central Universities, and the Australian Research Council (Grant Nos. FT190100188, LP230100278, DP240102628, and DP240102728)

Open access publishing facilitated by University of Southern Queensland, as part of the Wiley - University of Southern Queensland agreement via the Council of Australian University Librarians.

## Conflict of Interest

The authors declare no conflict of interest.

## Data Availability Statement

The data that support the findings of this study are available in the supplementary material of this article.

## Keywords

bioinspired, fire-retardant coating, group synergy, interface adhesion, self-healing

Received: July 18, 2024
Published online: August 30, 2024

[1] a) T. Li, J. Song, X. Zhao, Z. Yang, G. Pastel, S. Xu, C. Jia, J. Dai, C. Chen, A. Gong, *Sci. Adv.* **2018**, *4*, eaar3724; b) Z. L. Yu, N. Yang, V. Apostolopoulou-Kalkavoura, B. Qin, Z. Y. Ma, W. Y. Xing, C. Qiao, L. Bergstrom, M. Antonietti, S. H. Yu, *Angew. Chem. Int. Ed.* **2018**, *57*, 4538.

[2] a) B. W. Liu, H. B. Zhao, Y. Z. Wang, *Adv. Mater.* **2022**, *34*, 2107905; b) S. T. Lazar, T. J. Kolibaba, J. C. Grunlan, *Nat. Rev. Mater.* **2020**, *5*, 259.

[3] a) B. Yuan, G. Wang, S. Bai, P. Liu, *J. Appl. Polym. Sci.* **2019**, *136*, 47779; b) J. Huang, Z. Zhao, T. Chen, Y. Zhu, Z. Lv, X. Gong, Y. Niu, B. Ma, *Carbon* **2019**, *146*, 503.

[4] a) W. Zhao, H.-B. Zhao, J.-B. Cheng, W. Li, J. Zhang, Y.-Z. Wang, *Chem. Eng. J.* **2022**, *440*, 135807; b) M.-E. Li, Y.-W. Yan, H.-B. Zhao, R.-K. Jian, Y.-Z. Wang, *Compos. Pt. B-Eng.* **2020**, *185*, 107797; c) Q. Chen, J. Zhang, J. Li, J. Sun, B. Xu, H. Li, X. Gu, S. Zhang, *Polym. Degrad. Stab.* **2022**, *203*, 110079.

[5] a) L. Li, X. Shao, Z. Zhao, X. Liu, L. Jiang, K. Huang, S. Zhao, *ACS Omega* **2020**, *5*, 799; b) K. Li, Y. Li, Y. Zou, B. Yuan, A. Walsh, D. Carradine, *Fire Technol.* **2022**, *59*, 29.

[6] S. Hamdani-Devarennes, R. El Hage, L. Dumazert, R. Sonnier, L. Ferry, J. M. Lopez-Cuesta, C. Bert, *Prog. Org. Coat.* **2016**, *99*, 32.

[7] a) J. Reuter, T. Standau, V. Altstädt, M. Döring, *J. Fire Sci.* **2020**, *38*, 270; b) X. Shao, Y. Du, X. Zheng, J. Wang, Y. Wang, S. Zhao, Z. Xin, L. Li, *J. Mater. Sci.* **2020**, *55*, 7555.

[8] a) Z. Ma, X. Liu, X. Xu, L. Liu, B. Yu, C. Maluk, G. Huang, H. Wang, P. Song, *ACS Nano* **2021**, *15*, 11667; b) Z. Ma, J. Zhang, C. Maluk, Y. Yu, S. M. Seraji, B. Yu, H. Wang, *Matter* **2022**, *5*, 911; c) Z. Ma, J. Zhang, L. Liu, H. Zheng, J. Dai, L.-C. Tang, P. Song, *Compos. Commun.* **2022**, *29*, 101046.

[9] a) C. Leng, Y. Liu, C. Jenkins, H. Meredith, J. J. Wilker, Z. Chen, *Langmuir* **2013**, *29*, 6659; b) T.-P. Chen, T. Liu, T.-L. Su, J. Liang, *Langmuir* **2017**, *33*, 5863; c) J. Chen, H. Zeng, *Langmuir* **2022**, *38*, 12999; d) Y. Lee, K. Jun, K. Lee, Y. C. Seo, C. Jeong, M. Kim, I.-K. Oh, H. Lee, *Angew. Chem. Int. Ed.* **2020**, *59*, 3864; e) H. Yang, Y. Furutani, S. Kudo, J.-i. Hayashi, K. Norinaga, *J. Anal. Appl. Pyrolysis* **2016**, *120*, 321.

[10] J. Saiz-Poseu, J. Mancebo-Aracil, F. Nador, F. Busqué, D. Ruiz-Molina, *Angew. Chem. Int. Ed.* **2018**, *58*, 696.

[11] a) T. Yimyai, D. Crespy, M. Rohwerder, *Adv. Mater.* **2023**, *35*, 2300101; b) Y. Hou, G. Zhu, J. Cui, N. Wu, B. Zhao, J. Xu, N. Zhao, *J. Am. Chem. Soc.* **2021**, *144*, 436; c) Y. Hou, G. Zhu, S. O. Catt, Y. Yin, J. Xu, E. Blasco, N. Zhao, *Adv. Sci.* **2023**, *10*, 2304147.

[12] W. Zheng, H. Fan, L. Wang, Z. Jin, *Langmuir* **2015**, *31*, 11671.

[13] a) Y. Yang, J. Lyu, J. Chen, J. Liao, X. Zhang, *Adv. Funct. Mater.* **2021**, *31*, 2102232; b) Y. Guo, A. Baschieri, F. Mollica, L. Valgimigli, J. Cedrowski, G. Litwinienko, R. Amorati, *Angew. Chem. Int. Ed.* **2021**, *60*, 15220; c) W. Du, Z. Zhang, P. Li, L. Li, H. Huang, M. Yan, *J. Appl. Polym. Sci.* **2023**, *140*, e54500; d) J. H. Cho, V. Vasagar, K. Shanmuganathan, A. R. Jones, S. Nazarenko, C. J. Ellison, *Chem. Mater.* **2015**, *27*, 6784.

[14] a) A. Hanifpour, N. Bahri-Laleh, M. Nekoomanesh-Haghighi, *J. Appl. Polym. Sci.* **2020**, *138*, 49654; b) Z. Wang, H. Luo, L. Wang, H. Li, Y. Chen, J. Xiang, H. Fan, *Prog. Org. Coat.* **2023**, *182*, 107690.

[15] H. Cho, G. Wu, J. C. Jolly, N. Fortoul, Z. He, Y. Gao, A. Jagota, S. Yang, *Proc. Natl. Acad. Sci. USA* **2019**, *116*, 13774.

[16] a) Y. C. Li, S. Mannen, A. B. Morgan, S. Chang, Y. H. Yang, B. Condon, J. C. Grunlan, *Adv. Mater.* **2011**, *23*, 3926; b) D. D. Jiang, Q. Yao, M. A. McKinney, C. A. Wilkie, *Polym. Degrad. Stab.* **1999**, *63*, 423.

[17] B. Bingöl, W. H. Meyer, M. Wagner, G. Wegner, *Macromol. Rapid Commun.* **2006**, *27*, 1719.

[18] R. N. Walters, R. E. Lyon, *J. Appl. Polym. Sci.* **2002**, *87*, 548.

[19] a) R. E. Lyon, M. T. Takemori, N. Safronava, S. I. Stoliarov, R. N. Walters, *Polymer* **2009**, *50*, 2608; b) R. Sonnier, B. Otazaghine, L. Dumazert, R. Ménard, A. Viretto, L. Dumas, L. Bonnaud, P. Dubois, N. Safronava, R. Walters, R. Lyon, *Polymer* **2017**, *127*, 203; c) S. Wang, H. Jiang, R. Yu, S. Lou, L. Ma, J. Liu, T. Tang, *Chem. Mater.* **2022**, *34*, 8629.

[20] J. Cao, C. Lu, J. Zhuang, M. Liu, X. Zhang, Y. Yu, Q. Tao, *Angew. Chem. Int. Ed.* **2017**, *56*, 8795.

[21] X. Xu, L. Li, S. M. Seraji, L. Liu, Z. Jiang, Z. Xu, X. Li, S. Zhao, H. Wang, P. Song, *Macromolecules* **2021**, *54*, 9510.

[22] a) L. Liu, X. Xu, M. Zhu, X. Cui, J. Feng, Z. F. Rad, H. Wang, P. Song, *Adv. Mater. Technol.* **2023**, *8*, 2201414; b) X. Zhang, W. Liu, D. Yang, X. Qiu, *Adv. Funct. Mater.* **2019**, *29*, 1806912.

[23] a) J. Zhang, W. Wang, Y. Zhang, Q. Wei, F. Han, S. Dong, D. Liu, S. Zhang, *Nat. Commun.* **2022**, *13*, 5214; b) A. H. Hofman, I. A. van Hees, J. Yang, M. Kamperman, *Adv. Mater.* **2018**, *30*, 1704640; c) M. A. Rahman, C. Bowland, S. Ge, S. R. Acharya, S. Kim, V. R. Cooper, X. C. Chen, S. Irle, A. P. Sokolov, A. Savara, T. Saito, *Sci. Adv.* **2021**, *7*, eabk2451; d) H. Wang, X. Shi, Y. Xie, S. Gao, Y. Dai, C. Lai, D. Zhang, C. Wang, Z. Guo, F. Chu, *Cell Rep. Phys. Sci.* **2023**, *4*, 101374.

[24] G. Wang, W. Li, S. Bai, Q. Wang, *ACS Omega* **2019**, *4*, 9306.

[25] a) P. Yang, Z. Gu, F. Zhu, Y. Li, *CCS Chemistry* **2020**, *2*, 128; b) K. Y. Ju, Y. Lee, S. Lee, S. B. Park, J. K. Lee, *Biomacromolecules* **2011**, *12*, 625; c) H. Kim, D. W. Kim, V. Vasagar, H. Ha, S. Nazarenko, C. J. Ellison, *Adv. Funct. Mater.* **2018**, *28*, 1803172; d) V. Thavasi, L. P. Leong, R. P. A. Bettens, *J. Phys. Chem. A* **2006**, *110*, 4918.

[26] M. J. Hurley, D. T. Gottuk, J. R. Hall, K. Harada, E. D. Kuligowski, M. Puchovsky, J. L. Torero, J. M. Watts, C. Wieczorek, *SFPE Handbook of Fire Protection Engineering*, Springer, New York **2016**.

[27] L. Gu, Q. Yu, L. Zhang, *J. Appl. Polym. Sci.* **2020**, *137*, 49391.

[28] Z.-M. Zhu, Y.-J. Xu, W. Liao, S. Xu, Y.-Z. Wang, *Ind. Eng. Chem. Res.* **2017**, *56*, 4649.

[29] G. Wang, X. Chen, P. Liu, S. Bai, *J. Appl. Polym. Sci.* **2017**, *134*, 44356.

[30] W. Ji, D. Wang, J. Guo, B. Fei, X. Gu, H. Li, J. Sun, S. Zhang, *Carbohydr. Polym.* **2020**, *233*, 115841.
[31] S. P. Bhoite, J. Kim, W. Jo, P. H. Bhoite, S. S. Mali, K. H. Park, C. K. Hong, *Polymers* **2021**, *13*, 2662.
[32] S. Zhang, W. Ji, Y. Han, X. Gu, H. Li, J. Sun, *J. Appl. Polym. Sci.* **2018**, *135*, 46471.
[33] M.-E. Li, H.-B. Zhao, J.-B. Cheng, T. Wang, T. Fu, A.-N. Zhang, Y.-Z. Wang, *Engineering* **2022**, *17*, 151.
[34] W. Ji, Y. Yao, J. Guo, B. Fei, X. Gu, H. Li, J. Sun, S. Zhang, *J. Appl. Polym. Sci.* **2020**, *137*, 49045.
[35] J. Lu, D. Wang, P. Jiang, S. Zhang, Z. Chen, S. Bourbigot, G. Fontaine, M. Wei, *Constr. Build. Mater.* **2021**, *305*, 124773.
[36] Z. Wang, S. Jiang, H. Sun, *Iran. Polym. J.* **2016**, *26*, 71.
[37] B. Cao, X. Gu, X. Song, X. Jin, X. Liu, X. Liu, J. Sun, S. Zhang, *J. Appl. Polym. Sci.* **2017**, *134*, 44423.
[38] B. Cao, T. Yu, J. Sun, X. Gu, X. Liu, H. Li, B. Fei, S. Zhang, *J. Appl. Polym. Sci.* **2020**, *137*, 49227.
[39] L. Wang, C. Wang, P. Liu, Z. Jing, X. Ge, Y. Jiang, *Constr. Build. Mater.* **2018**, *176*, 403.
[40] a) J. Wang, L. Qian, Z. Huang, Y. Fang, Y. Qiu, *Polym. Degrad. Stab.* **2016**, *130*, 173; b) Y. Lu, J. Feng, D. Yi, H. Xie, Z. Xu, C.-F. Cao, S. Huo, H. Wang, P. Song, *Compos. Pt. A-Appl. Sci. Manuf.* **2024**, *176*, 107834.
[41] a) D. J. Morgan, *C-J. Carbon Res.* **2021**, *7*, 51; b) D. Q. Yang, B. Hennequin, E. Sacher, *Chem. Mater.* **2006**, *18*, 5033.
[42] W. Kumar, U. K. Sharma, M. Shome, *J. Constr. Steel Res.* **2021**, *181*, 106615.
[43] a) J. Chen, Z. Wang, B. Yao, Y. Geng, C. Wang, J. Xu, T. Chen, J. Jing, J. Fu, *Adv. Mater.* **2024**, *36*, 2401178; b) E. Immelman, R. D. Sanderson, E. P. Jacobs, A. J. Van Reenen, *J. Appl. Polym. Sci.* **1993**, *50*, 1013; c) A. Michele, P. Paschkowski, C. Hänel, G. E. M. Tovar, T. Schiestel, A. Southan, *J. Appl. Polym. Sci.* **2022**, *139*, e51606.
[44] M. Millaruelo, V. Steinert, H. Komber, R. Klopsch, B. Voit, *Macromol. Chem. Phys.* **2008**, *209*, 366.
[45] P. K. Sumit Sharma, R. Chandra, in *Molecular Dynamics Simulation of Nanocomposites Using BIOVIA Materials Studio, Lammps and Gromacs*, (Ed: S. Sharma), Elsevier, Amsterdam, Netherlands **2019**.
[46] T. Chakraborty, A. Hens, S. Kulashrestha, N. C. Murmu, P. Banerjee, *Physica E Low Dimens. Syst. Nanostruct.* **2015**, *69*, 371.